



Effects of climate variability on lake evaporation: Results from a long-term energy budget study of Sparkling Lake, northern Wisconsin (USA)

John D. Lenters^{a,*}, Timothy K. Kratz^b, Carl J. Bowser^c

^a*School of Environmental and Physical Sciences, Lake Superior State University, 650 W. Easterday Avenue, Sault Ste. Marie, MI 49783, USA*

^b*Center for Limnology, University of Wisconsin-Madison, Madison, WI, USA*

^c*Department of Geology and Geophysics, University of Wisconsin-Madison, Madison, WI, USA*

Received 7 October 2003; revised 20 September 2004; accepted 29 October 2004

Abstract

Variations in lake evaporation have a significant impact on the energy and water budgets of lakes. Understanding these variations and the role of climate is important for water resource management as well as predicting future changes in lake hydrology as a result of climate change. This study presents a comprehensive, 10-year analysis of seasonal, intraseasonal, and interannual variations in lake evaporation for Sparkling Lake in northern Wisconsin (USA). Meteorological and lake temperature measurements are made at a raft on the lake and are supplemented by radiation measurements from a nearby airport. The data are analyzed over 14-day periods from 1989 to 1998 (during the ice-free season) to provide bi-weekly energy budget estimates of evaporation rate (along with uncertainty estimates). The mean evaporation rate for Sparkling Lake over the study period is 3.1 mm day^{-1} , with a coefficient of variation of 25%. Considerable variability in evaporation rates is found on a wide range of timescales, with seasonal changes having the highest coefficient of variation (18%), followed by the intraseasonal (15%) and interannual timescales (12%; for summer means). Intraseasonal changes in evaporation are primarily associated with synoptic weather variations, with high evaporation events tending to occur during incursions of cold, dry air (due, in part, to the thermal lag between air and lake temperatures). Seasonal variations in evaporation are largely driven by temperature and net radiation, but are out-of-phase with changes in wind speed. This presents challenges when calculating evaporation rates by means of the simpler mass-transfer technique. On interannual timescales, changes in summer evaporation rates are strongly associated with changes in net radiation and show only moderate connections to variations in temperature or humidity. Nonetheless, we are able to identify a simple, empirical relationship for estimating interannual evaporation rates that is more accurate than the mass transfer technique.

© 2004 Elsevier B.V. All rights reserved.

Keywords: Evaporation; Lake; Energy budget; Climate; Water balance

* Corresponding author. Tel.: +1 906 635 2156; fax: +1 906 635 2266.

E-mail address: jlenters@lssu.edu (J.D. Lenters).

1. Introduction

1.1. Background

Lakes and reservoirs provide a valuable water resource that is important for irrigation, fishing and recreation, drinking water, aquatic ecosystems, transportation and commerce, and hydropower. The availability and quality of freshwater is, in turn, closely tied to variations in climate as well as direct human influences (e.g. Schindler, 2001). One of the most significant and broadly impacting effects of climate variability on lakes is changes in water level. Such changes reflect an alteration of the lake water balance, which can result from changes in: (1) precipitation over the lake and surrounding watershed, (2) land surface evapotranspiration and snowmelt (and associated surface runoff and/or groundwater flow), and/or (3) direct evaporation from the lake surface. It is crucial for water resource management, therefore, that the effects of climate variability on each of these hydrologic processes be well understood. Lake evaporation is somewhat unique in the sense that it is influenced not only by climate, but also by characteristics of the lake itself (e.g. depth, area, color/clarity, etc.). Furthermore, evaporation plays an important role not only in the water budget of a lake, but also in the energy budget. This introduces additional complexity through changes in water temperature and vertical mixing; effects which actually feedback onto evaporation itself. Even measuring evaporation accurately (within 10%) is a difficult task without significant investment in instrumentation and data processing (Winter et al., 2003; Winter, 1981). These practical and theoretical considerations impose significant challenges for lake evaporation studies (both observational and modeling), especially when considering long time periods and/or large lakes or regions (with varying climatic and lake characteristics). Despite these challenges, it is critical that accurate, long-term studies of lake evaporation be maintained in order to better understand variations in evaporation as well as the role of climate and potential impacts of climate change.

Observational studies of lake evaporation have used a variety of different methods to measure evaporation rates. These include the mass transfer, water balance, eddy correlation, and energy budget methods, as well

as others (Winter, 1981; Winter et al., 1995). The mass transfer method has been used in numerous studies (e.g. Yu and Knapp, 1985; Ikebuchi et al., 1988; Laird and Kristovich, 2002) as a result of its ease of application and suitability for modeling (e.g. Hostetler and Bartlein, 1990; Blodgett et al., 1997). Water balance studies, on the other hand (e.g. Myrup et al., 1979), can potentially provide a more reliable estimate of evaporation, so long as each water budget component is accurately measured (often a difficult task, especially for groundwater). In general, however, the energy budget and eddy correlation techniques are considered to be the most accurate methods, albeit at the cost of additional, high-quality instrumentation (Winter, 1981). Except for a recent study by Blanken et al. (2000), most applications of the eddy correlation technique have been confined to short-term studies (e.g. Sene et al., 1991; Stannard and Rosenberry, 1991), with the energy budget method being the preferred technique for accurate, long-term monitoring (e.g. Winter et al., 2003).

Despite this preference, the number of long-term (multi-year) energy budget studies of lake evaporation is rather limited (undoubtedly because of the labor and expense). Myrup et al. (1979) provide a review of some of the earlier studies of lake energy budgets, as well as their own 3-year analysis of the energy and water budgets of Lake Tahoe, California-Nevada (USA). A comprehensive, 10-year study of the energy budget of Perch Lake, Ontario (Canada) has been presented by Robertson and Barry (1985), while Sturrock et al. (1992) provide a 5-year analysis of energy budget evaporation rates for Williams Lake, Minnesota (USA). This latter study has also proven useful for evaluating alternative evaporation methods and instrumentation (Rosenberry et al., 1993; Winter et al., 1995). Sacks et al. (1994) present a brief (20-month), but interesting comparison of energy budget evaporation rates for two subtropical lakes of differing depth (in Florida, USA). dos Reis and Dias (1998) analyzed the energy budget of Lake Serra Azul (in southeastern Brazil) over a 2.5-year period and compared the evaporation results with estimates from the Complementary Relationship Lake Evaporation model (CRLE; Morton, 1983a,b, 1986). Vallet-Coulomb et al. (2001) performed a similar study of Lake Ziway (Ethiopia) over a 30-year period but made a number of simplifying assumptions in

the energy budget (e.g. constant Bowen ratio, equal air and lake surface temperatures, etc.). More recently, Winter et al. (2003) conducted a comprehensive 6-year energy budget analysis of evaporation rates for Mirror Lake, New Hampshire (USA).

Only four of these earlier studies (Robertson and Barry, 1985; Sturrock et al., 1992; Vallet-Coulomb et al., 2001; Winter et al., 2003) are long enough to provide robust estimates of variations in lake evaporation on a relatively wide range of timescales, including interannual variability. Despite this advantage, however, each of these studies remains somewhat limited in scope. Robertson and Barry (1985), for example, only briefly discuss the mean seasonal variability of lake evaporation and the interannual coefficient of variation, while Sturrock et al. (1992) present a more detailed but somewhat qualitative discussion of the long-term variability. Vallet-Coulomb et al. (2001), on the other hand, focus on the 30-year mean evaporation rate and have minimal discussion of the evaporation variability. Arguably, the most complete analysis of seasonal to interannual variations in lake evaporation is presented by Winter et al. (2003) for Mirror Lake. Nevertheless, the study is limited to six years, and discussion of climatic mechanisms focuses on radiation inputs, rather than a broad range of atmospheric influences. Furthermore, quantitative analysis of intraseasonal variations in evaporation is primarily limited to monthly timescales. As noted by Winter et al. (2003), this limitation is due to restrictions imposed by the length of time between lake thermal survey dates (which can vary widely within a season and from year to year).

The goal of the current study is to expand on this earlier work by providing a comprehensive, quantitative, energy-budget analysis of interannual, seasonal, and intraseasonal variations in lake evaporation, as well as the climatic mechanisms responsible for the variations. Although brief references are also made to the mass transfer method, a detailed application of this technique to Sparkling Lake is left for future work. Our study covers 10 full open-water seasons (roughly May–November; 1989–1998), and special care is taken to ensure that the energy-budget periods are the same from year-to-year so that variations in evaporation rate can be appropriately analyzed for each of the timescales under consideration. This report provides a complete description of the first set of

data to come out of this study, as well as a detailed methodology, extensive error analysis, and thorough discussion of the results and conclusions of the study.

1.2. Site description

The study site is Sparkling Lake, one of a suite of lakes being studied as part of the North Temperate Lakes Long-term Ecological Research Program (LTER; Magnuson and Bowser, 1990; Magnuson et al., 1997). Sparkling Lake is a 64-ha seepage lake located in Vilas County, northern Wisconsin (Fig. 1) and has been the subject of numerous hydrologic, geochemical, and ecological studies (Krabbenhoft et al., 1990a,b, 1992; Krabbenhoft and Webster, 1995; Hamilton and De Stasio, 1997; Hagerthey and Kerfoot, 1998). It is a clear, relatively deep, oligotrophic lake with a maximum depth of 20 m, mean depth of 10.9 m, mean Secchi disk depth of 6.1 m, and mean chlorophyll-a concentration of $2.2 \mu\text{g l}^{-1}$. Approximately 40 m of sandy tills and outwash overlie granitic bedrock in this region (Attig, 1985). Mixed deciduous/coniferous forest surrounds the lake. Sparkling Lake has no surface water inlets or outlets. For comparison with the Perch Lake, Williams Lake, and Mirror Lake evaporation studies (Robertson and Barry, 1985; Sturrock et al., 1992; Winter et al., 2003, respectively), Sparkling Lake is roughly twice as deep as Williams Lake and Mirror Lake and significantly deeper than Perch Lake (2 m mean depth). Sparkling Lake has also a larger surface area than the other three lakes (which range from 15 to 45 ha) and is located approximately 950 km west of Perch Lake (Ontario), 400 km east–southeast of Williams Lake (Minnesota), and 1400 km west of Mirror Lake (New Hampshire).

The climate in northern Wisconsin is humid continental with average annual, January, and July temperatures of 3.9, -13.3 , and 19.1 °C, respectively (1961–1990 data, Midwestern Regional Climate Center, Champaign, IL). Annual mean precipitation is 79 cm, with 62% falling during the five-month period from May through September. Additional aspects of the climate variability of the North Temperate Lakes region and other LTER sites are reviewed by Greenland and Kittel (2002). On average, Sparkling Lake is ice-free from April 22 through December 4 (based on the 1981–2001 mean). Similar to other rigorous studies of lake evaporation, a raft is

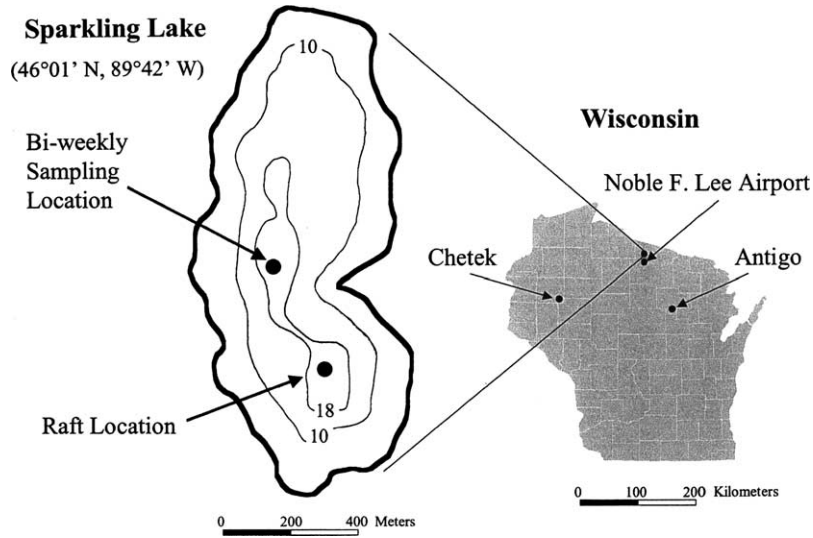


Fig. 1. Map of Sparkling Lake showing the bathymetry (10- and 18-m contours) and approximate locations of the meteorological raft and bi-weekly temperature profiles. Also shown is a map of Wisconsin (USA) indicating the location of the lake and three sites used for supplementary meteorological data (primarily radiation; see text).

maintained on the lake during the ice-free season in order to obtain the most accurate over-lake atmospheric measurements (Winter et al., 1995). Such measurements include air temperature, relative humidity, wind speed, and lake temperature (supplemented by bi-weekly sampling at a separate location; see Fig. 1 and Section 3). The raft is anchored at a deep location in the southern lobe of Sparkling Lake (Fig. 1) to facilitate complete lake temperature profiles and to maximize the fetch from the prevailing westerly to northwesterly winds. Supplementary meteorological measurements are available from three additional locations (Fig. 1; Section 3).

2. Methodology

2.1. Derivation of evaporation equation

The energy budget for a lake can be written as

$$\bar{R}_{\text{net}} + \bar{Q}_{\text{sed}} + \bar{A}_{\text{net}} - (\bar{E} + \bar{H}) = \bar{S}, \quad (1)$$

where R_{net} is net radiation, Q_{sed} is heat released by sediments, A_{net} is net heat advected into the lake, E and H are evaporative and sensible cooling, respectively, and S is the rate of change of heat stored in

the lake (due to temperature changes only; volumetric changes are accounted for in A_{net}). Overbars indicate temporal averaging over an appropriate timescale (14 days in this study), and all units are in W m^{-2} . Ice is not included in (1) since we are considering only the ice-free season in our analysis.

Net advected heat can be written as

$$A_{\text{net}} = A_{\text{P}} + A_{\text{GI}} - A_{\text{GO}} - A_{\text{E}} - A_{\text{L}}, \quad (2)$$

where the terms on the right-hand side of (2) refer to heat advected by precipitation (A_{P}), groundwater inflow (A_{GI}), groundwater outflow (A_{GO}), evaporation (A_{E}), as well as changes in heat storage due to variations in lake level (A_{L} ; originates from assuming a constant volume in S). River inflow and outflow are not considered since Sparkling Lake is a seepage lake and has negligible surface drainage. Advection of heat due to melting of snowfall is also ignored in this analysis. Each of the terms on the right-hand side of (2) can be written in the form

$$A_x = \rho_w c_w F_x (T_x - T_{\text{ref}}), \quad (3)$$

where ρ_w is the density of water (1000 kg m^{-3}), c_w is the specific heat of water ($4186 \text{ J kg}^{-1} \text{ }^\circ\text{C}^{-1}$), F_x is the flux (in m s^{-1}) of water by process x (i.e. precipitation, evaporation, groundwater, and change in lake level), T_x is the temperature of the water

(rain, groundwater, etc.), and T_{ref} is a reference temperature (usually 0 °C, but can be arbitrary if the lake water budget is closed: $F_P - F_E + F_{\text{GI}} - F_{\text{GO}} = F_L$).

If we now express groundwater outflow (F_{GO}) as a residual of the water budget and also assume $T_{\text{GO}} = T_L$ (since the exact depth and temperature of groundwater outflow are unknown¹), then (2) and (3) combine to produce

$$A_{\text{net}} = \rho_w c_w [F_P(T_P - T_L) + F_{\text{GI}}(T_{\text{GI}} - T_L) - F_E(T_E - T_L)]. \quad (4)$$

Note that $F_E = E/\rho_w L_v$, where E , as given earlier, is the evaporation rate in W m^{-2} , and L_v (assumed constant at $2.46 \times 10^6 \text{ J kg}^{-1}$) is the latent heat of vaporization. Also, T_E is equal to T_s , the surface temperature of the lake, and so (4) becomes

$$A_{\text{net}} = A_0 - c_w E(T_s - T_L)/L_v, \quad (5)$$

where

$$A_0 = \rho_w c_w [F_P(T_P - T_L) + F_{\text{GI}}(T_{\text{GI}} - T_L)]. \quad (6)$$

Finally, writing the sensible cooling term in (1) as $\bar{H} = \bar{E}B$, where B is the Bowen ratio, combining (5) with (1), and solving for \bar{E} , we get

$$\bar{E} = \frac{\bar{R}_{\text{net}} - \bar{S} + \bar{Q}_{\text{sed}} + \bar{A}_0}{1 + B + c_w(\bar{T}_s - \bar{T}_L)/L_v}, \quad (7)$$

which is our governing equation for calculating evaporation rate. Note that in deriving (7) it has been assumed that $\overline{E(T_s - T_L)} \approx \bar{E}(\bar{T}_s - \bar{T}_L)$. This is not a critical assumption (Webb, 1960) given that the last additive term in the denominator of (7) is relatively insignificant (in the order of 10^{-2}). Similar temporal correlations are also ignored in calculating \bar{A}_0 (Eq. (6)).

2.2. Energy budget components

Net radiation in (7) is calculated from

$$\bar{R}_{\text{net}} = \bar{R}_{\text{swd}}(1 - \alpha_{\text{sw}}) + \bar{R}_{\text{lwd}}(1 - \alpha_{\text{lw}}) - \bar{R}_{\text{lwu}}, \quad (8)$$

¹ T_L (as calculated in the derivation of A_L) is the area-averaged temperature of lake water in contact with sediment and, therefore, is more heavily weighted towards shallow waters, where groundwater outflow typically occurs.

where R_{swd} is downward shortwave radiation, $\alpha_{\text{sw}} = 0.07$ is the shortwave albedo of water (value taken from Budyko, 1974), R_{lwd} is downward longwave radiation, $\alpha_{\text{lw}} = 0.03$ is longwave albedo (Brutsaert, 1982), and $R_{\text{lwu}} = \varepsilon \sigma T_s^4$ is upward (emitted) longwave radiation. ($\varepsilon = 0.97$ is the emissivity of water, and $\sigma = 5.67 \times 10^{-8} \text{ W m}^{-2} \text{ K}^{-4}$ is the Stefan–Boltzman constant.)

The 14-day mean heat storage term in (7) is calculated from

$$\bar{S} = \frac{\rho_w c_w}{\bar{a}_s} \sum_z \left(\frac{\Delta T(z)}{\Delta t} a(z) \Delta z \right), \quad (9)$$

where a_s is lake surface area, $\Delta T(z) = T_{t+7}(z) - T_{t-7}(z)$ is the 14-day (centered) change in daily mean lake temperature at depth z , $\Delta t = 14$ days (converted to seconds), $a(z)$ is lake area at depth z , and Δz is layer thickness (typically 1 m). Lake area is estimated from a hypsometric curve of Sparkling Lake (generated from a bathymetric map) in conjunction with lake level data (available roughly every 2 weeks). Although explicitly accounted for, temporal changes in lake surface area and mean depth are relatively small over the 10-year period of record ($\pm 4\%$ and $\pm 1\%$ of the long-term mean, respectively).

The sediment heating term, \bar{Q}_{sed} , is estimated using a sinusoidal heat flux equation derived from Likens and Johnson (1969). This method only estimates the average seasonal cycle of sediment heat flux and does not, therefore, account for interannual or intraseasonal variations. The amplitudes of the average annual temperature cycle and average date of maximum water temperature at each depth were estimated for Sparkling Lake and used to calculate the depth-dependent sediment heating. This was then integrated over the depth of the lake (more precisely, sediment area) to calculate \bar{Q}_{sed} , which can be approximated by the following function

$$\bar{Q}_{\text{sed}} = \gamma + \beta \cos[\omega(\tau - \delta)], \quad (10)$$

where $\gamma = 0.24 \text{ W m}^{-2}$, $\beta = 5.3 \text{ W m}^{-2}$, $\omega = 2\pi/365$, $\tau = \text{day of year}$, and $\delta = 358$. Values for sediment thermal conductivity ($1.2 \text{ W m}^{-1} \text{ }^\circ\text{C}^{-1}$) and specific heat per unit volume ($1.0 \text{ cal cm}^{-3} \text{ }^\circ\text{C}^{-1}$) were unavailable for Sparkling lake and are based on

estimates from Likens and Johnson (1969) and Rogers et al. (1995).

The \bar{A}_0 advection term (Eq. (6)) has been explicitly calculated for the first 7 years of the analysis (1989–1995) using 14-day running mean precipitation data from nearby stations and bi-weekly lake level data. F_{GI} is estimated as a residual from the water budget² after assuming a constant groundwater outflux of $F_{GO} = 52 \text{ cm yr}^{-1}$ ($1.6 \times 10^{-8} \text{ m s}^{-1}$). (Any negative values of F_{GI} are assigned to F_{GO} as additional outflux.) The constant value for F_{GO} is based on stable isotope and numerical modeling estimates from Krabbenhoft et al. (1990a,b), who note that groundwater outflux for Sparkling Lake is much less variable than influx. Subsequent corrections to the numerical estimates (Krabbenhoft et al., 1992) indicate that groundwater outflux may be as large as 64 cm yr^{-1} . Wet-bulb temperature is used for T_p (Eq. (6)), while T_{GI} is estimated from the average seasonal cycle of groundwater temperature (mean = $9.3 \text{ }^\circ\text{C}$, range = $5.7 \text{ }^\circ\text{C}$). This estimate is based on five years of monthly groundwater temperature data collected at nearby wells by the United States Geological Survey (USGS; David Hamilton, personal communication). Using these inputs, \bar{A}_0 was found to never exceed 3.2 W m^{-2} in absolute value, with a mean value of 0.1 W m^{-2} and standard deviation of 0.7 W m^{-2} . This is considerably less than other components of the energy budget—too small, in fact, to warrant rigorous calculation of \bar{A}_0 for the full 10 years (and future time periods). Thus, to reduce unnecessary complexity, we simply assume \bar{A}_0 to have a constant value of 0.1 W m^{-2} (and estimated maximum uncertainty of $\pm 1.4 \text{ W m}^{-2}$). Despite this simplification, it is important to note that the above analysis was necessary to provide reasonable estimates of the error associated with assuming a constant \bar{A}_0 . Sturrock et al. (1992) also found temperature advection from groundwater and precipitation to be minor contributors to the energy budget of Williams Lake (generally less than 5 W m^{-2}), as did Winter et al. (2003) for Mirror Lake (less than 10 W m^{-2}). This is an important distinction from the water budget, since precipitation and groundwater each contribute

significantly to the net water flux of each of these lakes (Krabbenhoft et al., 1990b; Sturrock et al., 1992; Winter et al., 2003).

The Bowen ratio in (7) is calculated according to dos Reis and Dias (1998)

$$B = \frac{p_a c_{pa}}{0.622 L_v} \frac{U(T_s - T_a)}{U[e_s(T_s) - RH \times e_s(T_a)]} \quad (11)$$

where p_a is atmospheric pressure, c_{pa} is the specific heat of air at constant pressure ($1011 \text{ J kg}^{-1} \text{ }^\circ\text{C}^{-1}$), U is wind speed, T_a is air temperature, $e_s(T)$ is saturation vapor pressure at temperature T , and RH is relative humidity. Atmospheric pressure is assumed constant at $9.58 \times 10^4 \text{ Pa}$, based on data for Green Bay, Wisconsin (corrected for elevation). Most energy budget studies ignore temporal correlations with wind speed and simply allow U to drop out of Eq. (11). However, as noted by Webb (1960), the resulting impact on evaporation estimates can be non-trivial. In the present study we calculate B based on (11) and daily-mean measurements of U , T_s , T_a , and RH.

Since reliable hourly data are not available for the full 10 years of our study, we account for hourly covariances in (11) by writing the Bowen ratio (similar to Webb, 1964) as

$$B = k_1 B_d + k_2, \quad (12)$$

where B_d is the Bowen ratio using daily measurements (Eq. (11)) and k_1 and k_2 are empirical constants. Based on data for 1989–1992 (for which we have accurate hourly estimates of U , T_s , T_a , and RH), a piecewise linear regression between B and B_d results in the following estimates for k_1 and k_2 :

$$k_1, k_2 = \begin{cases} 1.45, & -0.15 : B_d \leq 0.2, \\ 1.075, & -0.075 : B_d \geq 0.2. \end{cases} \quad (13)$$

Thus, except for large Bowen ratios ($B_d \geq 1$), B is generally lower than B_d , resulting in lower sensible cooling rates and higher evaporation. This primarily reflects the positive (negative) diurnal correlation between air temperature and wind speed (relative humidity), particularly in the springtime (when Bowen ratios are low). Similar to the results of Webb (1960), we find that the correction for hourly covariances (Eq. (12)) increases 14-day evaporation estimates by an average of 5% (over the period 1989–1998), with a range of -1 to $+25\%$. Daily covariances have a

² For the purposes of the water budget, E was calculated from (7) under the assumption $A_0 = 0$.

similarly important impact on calculated evaporation rates. For example, if daily wind speed is allowed to drop out of Eq. (11), the resulting change in evaporation ranges from -11 to $+29\%$ (with a mean bias of 1% and standard deviation of 3%). These daily covariances are due to the characteristics of synoptic weather variability, such as the passage of a cold front (cool, windy conditions). Regardless of the cause, it is clear that diurnal and daily covariances can have a significant influence on the Bowen ratio and resulting evaporation rates for Sparkling Lake. This is somewhat different from the results of dos Reis and Dias (1998), who found little difference between Bowen ratios calculated from hourly, daily, or even monthly mean inputs. Their study, however, was performed over a considerably shorter timescale (5 days, in the case of the hourly data) and in a tropical, rather than mid-latitude location.

3. Data sources and quality

3.1. General information

Eq. (7) (together with Eqs. (8)–(13) and $\bar{A}_0 = 0.1 \text{ W m}^{-2}$) is used to calculate the 14-day running

mean evaporation rate. Measured variables (see Table 1) include downward radiation (shortwave and longwave), lake level and temperature profiles, air temperature, relative humidity, and wind speed. Atmospheric variables are measured at the raft on Sparkling Lake, while radiation measurements are made at the Noble F. Lee Municipal Airport (roughly 9 km southwest of the lake; Fig. 1). Lake level and temperature surveys are performed on Sparkling Lake on a roughly bi-weekly basis and are supplemented by daily-averaged water temperature measurements on the raft.

Aside from the lake surveys, all measurements are made at 1-min intervals and averaged to daily. Further averaging to 14-day running means is performed to be consistent with the temperature surveys as well as to provide a robust timescale for application of the energy budget technique (Winter, 1981; Winter et al., 2003). (The 14-day means are centered on day 8, with days 1 and 15 weighted by 50% to result in a 14-day average. This averaging scheme, which essentially approximates a beginning and ending time of 12:00 local time, is meant to coincide with the 14-day change in daily mean lake temperature in Eq. (9).) The raft has been deployed on Sparkling Lake since 1989 and remains on the lake for the majority of the ice-free

Table 1

List of primary variables along with their mean value and standard deviation (calculated over the entire 1519 14-day running mean samples during the 10 summers, 1989–1998). Also shown are the percent data filled with auxiliary measurements, maximum error estimates, and the corresponding error in evaporation rate. Variables are listed in order of decreasing %E error

Variable	Definition	Mean	SD	Filled (%)	Max. error	E error (%)
R_{ldw}	Downward LW radiation	342 W m^{-2}	28 W m^{-2}	40.7	2% (+10 W m^{-2}) ^a	10.5
R_{swd}	Downward SW radiation	185 W m^{-2}	56 W m^{-2}	13.2	2% (+28 W m^{-2}) ^a	9.2
S	Lake heat storage rate	-6.4 W m^{-2}	56 W m^{-2}	1.0	10 (2.3 W m^{-2}) ^b	9.2 (2.1 ^b)
T_s	Lake surface temperature	18.3 °C	4.2 °C	1.0	0.5 °C	5.1
RH	Relative humidity	78.7%	6.4%	47.3	7% RH	4.2
B	Bowen ratio	0.25	0.19	–	0.047	4.0
T_a	Air temperature	14.8 °C	5.0 °C	1.2	0.5 °C	3.3
α_{sw}	Shortwave albedo	0.07	–	–	20%	2.6
α_{lw}	Longwave albedo	0.03	–	–	20%	1.9
Q_{sed}	Sediment heat flux	-2.3 W m^{-2}	2.7 W m^{-2}	–	2.0 W m^{-2}	1.8
A_0	Advective heat flux	0.1 W m^{-2}	0.7 W m^{-2}	–	1.4 W m^{-2}	1.3
U	Wind speed	2.3 m s^{-1}	0.45 m s^{-1}	2.3	0.5 m s^{-1}	0.5
E	Evaporation rate	89.0 W m^{-2}	22.3 W m^{-2}	–	–	–
H	Sensible heat flux	20.8 W m^{-2}	13.4 W m^{-2}	–	–	–
R_{lwu}	Upward LW radiation	397 W m^{-2}	22 W m^{-2}	–	–	–
R_{net}	Net radiation	107 W m^{-2}	55 W m^{-2}	–	–	–

^a If auxiliary data is used.

^b Summer average (14 weeks).

season. Here, we present results from 10 years of data collection (1989–1998). Aside from 1998, which had an unusually warm winter and spring, the earliest date of raft deployment is May 3, while the latest date of removal is November 18. Thus, the analysis for each of the ten years is restricted to this 200-day period. Taking into consideration data gaps early or late in the season (when the raft was not deployed), this leads to a total of 1519 days for which an estimate of the 14-day running mean evaporation rate is available.

3.2. Radiation data

Downward shortwave radiation is measured at the airport using an Eppley PSP pyranometer³. Occasional missing or bad data (Table 1) is filled with radiation data from Antigo or Chetek, Wisconsin (roughly 97 and 157 km from the airport, respectively; Fig. 1). Data from these two stations are first adjusted using regressions with the airport radiation data. In addition, seven days of missing shortwave radiation data (one in 1989 and six in 1996, usually non-consecutive) were filled with linear interpolation, because no auxiliary data were available for these dates.

Incoming longwave radiation is measured with an Eppley PIR radiometer. Missing or faulty data (Table 1) are filled using an empirical method described by Brutsaert (1982). This method utilizes measurements of air temperature, humidity, and cloudiness to estimate downwelling longwave radiation. Here, we use temperature and humidity measurements from the raft and estimate cloudiness from the shortwave radiation data (relative to a theoretical clear sky). We find that this method provides longwave radiation estimates which are in very good agreement with the observations ($R^2 > 0.8$). There is, however, a slight bias in the empirical estimates, which we correct using regressions against data for 1989–1995. Observed longwave radiation data for 1996 and 1997 were found to have erroneously high readings and were replaced entirely with the empirical estimates.

3.3. Lake temperature data

The bi-weekly surveys (Fig. 1) measure lake temperature at 19 depths (from 0 to 18 m at 1-m intervals) using YSI thermistors. We also interpolate to 0.5-m depth (where we have daily estimates from the raft), resulting in a total of 20 depths. The ‘bi-weekly’ sampling interval actually varies in length from about 12 to 16 days and does not lie on the same date year to year. To overcome the difficulties this would impose on the analysis, as has been encountered in previous studies (e.g. Winter et al., 2003), we supplemented the bi-weekly temperatures with data from an additional thermistor chain which is monitored continuously from the raft (sampled every minute and averaged to daily means). In contrast to the bi-weekly surveys, the raft-based thermistor chain measures temperatures at only eight depths (from 0 to 12 m at 0.5- to 2-m intervals). Furthermore, some of these continuously-monitored thermistors were found to be unreliable during portions of the 10-year deployment and often showed a mean bias in comparison with the more accurate bi-weekly surveys. Although these shortcomings prevented us from using the raft-based temperatures exclusively, the measured daily *variability* was deemed to be quite realistic (certainly more so than a simple linear interpolation between bi-weekly surveys). Therefore, we were able to combine the accuracy of the bi-weekly surveys with the higher sampling frequency of the raft measurements to create a ‘merged’ temperature dataset. Specifically, a time-varying correction term was added to the daily raft-based temperatures so that at the bi-weekly sampling dates, the temperatures were identical to those measured by the surveys. ‘In-between dates’ were adjusted in a similar fashion, with the correction term varying linearly from one bi-weekly sampling date to the next. Following the adjustment process, any missing daily data were simply filled with standard linear interpolation. Such data gaps primarily occur below 12 m, where no daily data are available. Temperature changes below 12 m, however, are much smaller (and more linear) than at shallower depths, so this is not likely to have a large impact. Finally, small corrections were made to the temperature profiles to eliminate density inversions and provide more

³ Brand names are mentioned here for information purposes only and do not indicate an endorsement of the product.

realistic estimates of deep-water temperature changes during fall turnover.

This merged water temperature dataset provides a much better estimate of daily water temperature than either of the two raw datasets would provide individually. More importantly, it provides a means of obtaining a uniform analysis interval (14 days) for calculating the heat storage term (Eq. (9)). This allows one to compare seasonal to interannual variations in evaporation rate in a much more consistent manner than has been done in previous studies. Note that although some errors in daily water temperature are likely to remain following the merging process, they are minimized by the fact that the storage term is calculated based on a 14-day difference in water temperature. Also, the use of only one or two sampling locations for estimating mean lake temperature profiles is not likely to lead to significant errors in calculated evaporation rates for a lake of this size (Crow and Hottman, 1973; Rosenberry et al., 1993).

3.4. Air temperature, relative humidity, and wind speed

Air temperature and relative humidity are measured at the raft at a height of 2 m using a Campbell Scientific 207 probe mounted within a radiation shield. Missing or bad data (Table 1) are filled with data from the municipal airport (regressed and adjusted against the raft data), with the exception of 1993, which utilized auxiliary data from a wet/dry bulb humidity sensor (mounted on the raft). In general, we found the relative humidity data to be the least reliable of all the data sources and were forced to use only auxiliary data for the years 1993–1996 and 1998. (The solid-state sensor had a tendency to drift toward low humidity values, particularly toward the end of the deployment season.) Despite these uncertainties in relative humidity, the resulting impact on energy budget-derived evaporation rates is rather small (see Table 1 and Section 3.5).

Wind speed is measured at the raft at a height of 2 m using a Gill 3-cup anemometer from RM Young (model 12102). Back-up anemometers are also mounted at 1 and 3 m and supplementary data are available from the airport as well.

3.5. Uncertainty analysis

Given the uncertainties in the input data, particularly those using secondary data sources, it is important to provide an error analysis of the resulting evaporation estimates (Winter, 1981; Rosenberry et al., 1993). Table 1 provides a list of the various input variables, their estimated maximum uncertainties, the percentage of days filled with auxiliary data, and the associated error in evaporation rate (as a percentage of the 10-year mean evaporation). Variables are listed in order of highest to lowest impact on evaporation error. Also shown in Table 1 are the 10-year averages and standard deviations of the 14-day running mean input variables and various calculated quantities (such as evaporation). Most of the uncertainties in input variables are based on manufacturer specifications or rough estimates. Net error in the lake storage term was determined by statistically summing individual thermistor errors over the lake column (combined with small errors in lake level and hypsometry). Additional uncertainty was added to R_{lwd} , R_{swd} , S , T_s , and RH to account for the use of auxiliary data (and water temperature corrections). In most cases (as in Sacks et al., 1994), these additional uncertainties are based on the standard error of regression between primary and auxiliary data. Similar means were used to arrive at error bounds for Q_{sed} , A_0 , and B . (The uncertainty in B listed in Table 1 accounts only for the empirical approximation of hourly covariances given in Eq. (12). Additional errors in B are accounted for by uncertainties in T_s , T_a , RH, and U .)

The maximum likely error in evaporation rate associated with each variable was estimated by calculating the 14-day running mean E with and without the uncertainties listed in Table 1 (both positive and negative). The RMS difference in E (over the 10-year period) was then assigned as the associated error (Table 1). Because the uncertainty estimates were applied as a mean bias, it is possible that evaporation errors associated with the daily covariance terms (U , T_s , T_a , and RH) are underestimated. However, large variations in measurement error within a 14-day period are rather unlikely, so it is reasonable to assume that the error estimates in Table 1 represent upper bounds.

Similar to previous studies, we find that uncertainties in incoming shortwave and, especially, longwave radiation represent the largest sources of error in calculated evaporation rates (Table 1). Associated maximum evaporation errors average around 10%, which is higher than other estimates in the literature (typically 5% or less; e.g. Winter, 1981; Sacks et al., 1994). This is primarily because we have included uncertainties associated with auxiliary data and have assumed a maximum instrument error of 2% (somewhat higher than previous studies). Uncertainties in the storage term affect evaporation rates as much as incoming shortwave radiation, but the impact decreases to roughly 2% as the averaging period increases to 14 weeks (Table 1). Maximum errors in the remaining variables affect evaporation rates by 5% or less. Note that surface temperature affects upwelling radiation as well as the Bowen ratio, so errors in T_s are potentially offsetting. Also, relative humidity only affects the partitioning between latent and sensible cooling, the latter being generally smaller than the former. Thus, despite the high uncertainty in RH, the impact on evaporation rate is less than half that of radiation.

To combine the uncertainties listed in Table 1 and thereby provide net error bars for evaporation (and other calculated quantities), a Monte Carlo technique is employed. The 14-day mean evaporation rate (Eq. (7)) is calculated 1000 times for each day of the 10-year period. During the 1000 iterations, the 12 input parameters (Table 1) are assigned errors chosen randomly from normal distributions. The distributions have a mean of zero and a standard deviation equal to half the maximum uncertainty listed in Table 1. The standard deviation of the resulting 1000 evaporation estimates is then used to define, for each day, the RMS uncertainty in 14-day mean evaporation. Over the 10-year period, the median (maximum) RMS uncertainty is equal to 6.9 W m^{-2} (19.6 W m^{-2}), or roughly 7.8% (22%) of the mean evaporation rate (Table 1). In the sections that follow, we use a more conservative uncertainty estimate of twice the standard deviation (i.e. roughly 95% confidence intervals) to represent maximum error bounds. Thus, the 14-day mean evaporation estimates, on average, have a 95% likelihood of being within 16% of their true value. This is comparable to previous energy budget evaporation studies, which generally estimate error bounds to be

around 10–15% (Winter, 1981; Sturrock et al., 1992; Sacks et al., 1994; Winter et al., 2003).

4. Results

4.1. Evaporation rate and mean energy budget

Fig. 2 shows the 14-day running mean evaporation rate for 1989–1998 as calculated from Eq. (7). A wide range of variability is exhibited, from a maximum of 158 W m^{-2} (5.6 mm day^{-1}) during 5–19 August 1989 to a minimum of 34 W m^{-2} (1.2 mm day^{-1}) during 10–24 September 1994. The mean evaporation rate (Table 1) for the entire period is 89 W m^{-2} (3.1 mm day^{-1}), with a standard deviation of 22 W m^{-2} (0.8 mm day^{-1}). This evaporative heat flux combines with a sensible flux of 21 W m^{-2} to produce a net cooling of 110 W m^{-2} at the lake surface and an overall Bowen ratio of 0.23 (0.25 if calculated as an average of the ratios⁴). Most of the surface cooling is balanced by net radiation (107 W m^{-2}) which, in turn, is dominated by absorbed solar radiation (172 W m^{-2}). Incoming and outgoing longwave fluxes are large (Table 1), but opposite in sign, leading to a net loss of longwave radiation of 65 W m^{-2} . The small imbalance between the radiative and surface fluxes, combined with cooling from net advection and sediment heat fluxes, leads to an average lake cooling of 6.4 W m^{-2} during the overall sampling period.

The variations in evaporation rate shown in Fig. 2 are found to span a broad range of temporal scales. For example, a seasonal cycle is clearly evident in many years, with low evaporation rates in spring followed by high evaporation in summer and low values in autumn. Interannual variations are also evident, with high evaporation rates in 1989 and 1998 and low amounts in 1992 and 1994. Finally, significant short-term variations in evaporation (on roughly 14- to 30-day timescales) are seen in Fig. 2 as well. Particularly dramatic examples of this occur in 1993 and 1998, when evaporation rates change by up to a factor of

⁴ Subsequent references to multi-year or summer ‘mean Bowen ratios’ refer to averages of the 14-day Bowen ratios, not ratios of the average fluxes. The distinction, while important, leads to only small numerical differences in this study.

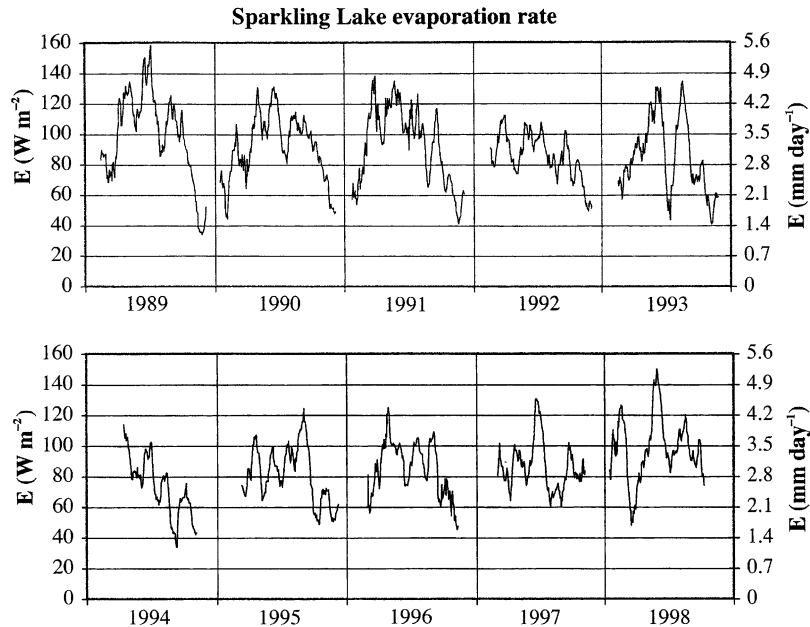


Fig. 2. Sparkling Lake evaporation rates for 1989–1998. The data represent centered, 14-day running means and are calculated using the energy budget method. Only the 200-day period of May 3–November 18 is shown for each year (with some missing data at the beginning and end of each year). Units are expressed in both W m^{-2} and mm day^{-1} .

three in as little as two weeks. These strong intraseasonal variations significantly modify the underlying seasonal variability, indicating that one cannot assume that lake evaporation for a particular year will simply follow an ‘average’ seasonal cycle. This result was also found by Sturrock et al. (1992) and Winter et al. (2003) in energy budget studies of Williams Lake and Mirror Lake, respectively.

Given the significant evaporation variability on each of these three timescales, the remainder of the analysis is partitioned into three sections: (1) seasonality, (2) interannual variability, and (3) short-term variations. Appropriate averaging is performed to highlight the various timescales. In order to simplify the analysis, we have sampled the various 14-day running mean timeseries once every 14 days to create a bi-weekly dataset that is non-overlapping in time (aside from 50% weighting at the tails). The 13 bi-weekly periods (listed in Table 2) are the same, year to year, and were chosen in such a way that the total number of periods for which data are available is maximized (110 out of a possible 130). The selected sampling periods also avoid two short episodes in 1991 when the 14-day evaporation rates are highly

uncertain (due to negative Bowen ratios). The resulting maximum error bounds of the 110 sampling periods range from 9 to 42% (of the respective 14-day mean evaporation), with a median value of 16% and standard deviation of 6%. When averaged over an entire summer (the seven bracketed periods in Table 2), the maximum error drops to a median value of 12%. It should be kept in mind that, since these uncertainty estimates represent maximum bounds, the *actual* errors in evaporation rate are likely to be considerably less than these upper bounds.

4.2. Seasonal variability

Fig. 3 and Table 2 show the mean seasonal energy budget of Sparkling Lake (averaged over the number of years listed in Table 2). Following Eq. (1), evaporative and sensible cooling are shown as negative values in Fig. 3 such that, when added to the net radiation (R_{net}) and sediment/advection terms ($Q_{\text{sed}} + A_{\text{net}}$), one is left with the heat storage term (S). Net radiation shows considerable seasonal variation, reaching a maximum of 159 W m^{-2} during the period 21 June–5 July and dropping off significantly

Table 2

List of 13 bi-weekly energy budget periods selected for study and the number of years with available data. Also shown are the mean energy budget components for each bi-weekly period (averaged over the number of years shown) as well as the overall, 26-week mean and standard deviation. Start and end dates for each 2-week period are weighted by 50% to produce a centered, 14-day average. The periods in italics (4–10) have 10 complete years of data and are utilized for further analysis of the interannual and intraseasonal variability. Variables are defined in Table 1.

Period	Start	End	No. of years	E (mm day ⁻¹)	E (W m ⁻²)	R_{net} (W m ⁻²)	S (W m ⁻²)	H (W m ⁻²)	B
1	10-May	24-May	2	2.91	82.8	146.6	55.0	4.1	0.10
2	24-May	7-Jun	6	3.07	87.4	150.9	39.9	18.1	0.20
3	7-Jun	21-Jun	9	2.85	81.2	153.2	57.8	8.2	0.09
4	<i>21-Jun</i>	<i>5-Jul</i>	<i>10</i>	<i>3.46</i>	<i>98.6</i>	<i>158.9</i>	<i>42.1</i>	<i>11.7</i>	<i>0.12</i>
5	<i>5-Jul</i>	<i>19-Jul</i>	<i>10</i>	<i>3.46</i>	<i>98.5</i>	<i>156.1</i>	<i>36.0</i>	<i>15.3</i>	<i>0.16</i>
6	<i>19-Jul</i>	<i>2-Aug</i>	<i>10</i>	<i>3.82</i>	<i>108.8</i>	<i>146.5</i>	<i>13.7</i>	<i>18.0</i>	<i>0.17</i>
7	<i>2-Aug</i>	<i>16-Aug</i>	<i>10</i>	<i>3.55</i>	<i>101.2</i>	<i>130.7</i>	<i>5.0</i>	<i>19.6</i>	<i>0.19</i>
8	<i>16-Aug</i>	<i>30-Aug</i>	<i>10</i>	<i>3.21</i>	<i>91.3</i>	<i>116.0</i>	<i>5.4</i>	<i>15.5</i>	<i>0.18</i>
9	<i>30-Aug</i>	<i>13-Sep</i>	<i>10</i>	<i>3.38</i>	<i>96.3</i>	<i>86.6</i>	<i>-38.1</i>	<i>26.0</i>	<i>0.27</i>
10	<i>13-Sep</i>	<i>27-Sep</i>	<i>10</i>	<i>3.05</i>	<i>86.8</i>	<i>57.1</i>	<i>-63.4</i>	<i>32.9</i>	<i>0.38</i>
11	27-Sep	11-Oct	9	2.66	75.8	38.0	-66.9	30.0	0.40
12	11-Oct	25-Oct	9	2.17	61.9	20.1	-70.8	31.4	0.50
13	25-Oct	8-Nov	5	1.83	52.1	-9.1	-102.9	45.2	0.85
Mean				3.03	86.4	104.0	-6.7	21.2	0.28
SD				0.56	16.0	58.8	54.9	11.4	0.21

thereafter (below zero after 25 October). This pattern is closely mimicked by changes in the heat storage term, which maximizes roughly two weeks prior to net radiation and drops off at a similar rate thereafter (Fig. 3). The transition from net warming of Sparkling Lake to net cooling occurs in late August to early September (on average).

Although the timing of the net radiation and heat storage terms is quite similar, there are important differences that translate into variations in evaporative and sensible cooling. For example, note that during the months of June and July the heat storage term drops off more rapidly than net radiation (Fig. 3, Table 2). This indicates an increase in evaporative

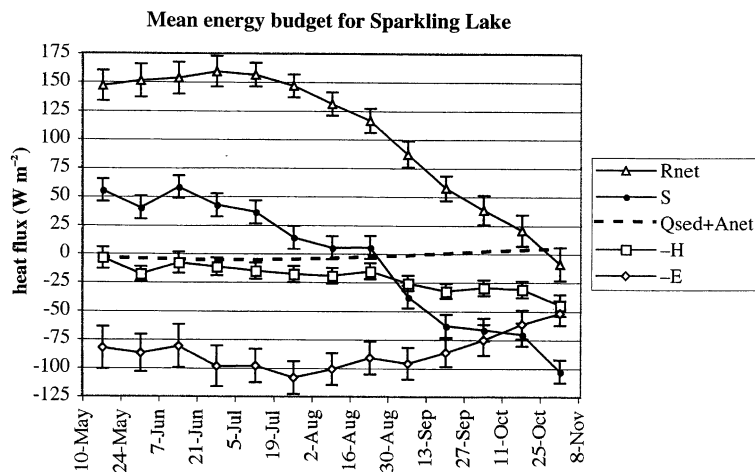


Fig. 3. Mean energy budget for Sparkling Lake for each of the 13 bi-weekly periods (averaged over the number of years indicated in Table 2). Heat flux components include net radiation (R_{net}), heat storage rate (S), and sediment and advective heat fluxes ($Q_{sed} + A_{net}$). Sensible and evaporative cooling rates are expressed as negative quantities ($-H$ and $-E$, respectively). Units are in $W m^{-2}$, and error bars indicate the estimated maximum uncertainty (not shown for $Q_{sed} + A_{net}$).

cooling, which maximizes in late July, roughly one month after net radiation. Evaporation begins to drop off in August and, by early November, is less than half the maximum summer value (Table 2). These seasonal changes in evaporation and radiation are similar to what has been found in previous energy budget studies of north temperate lakes (Myrup et al., 1979; Robertson and Barry, 1985; Sturrock et al., 1992; Winter et al., 2003). The sensible cooling term (Fig. 3) exhibits much different seasonal behavior and simply shows a general increase in cooling as the season progresses. By September, sensible cooling rates are roughly twice that of the spring and summer values (Table 2). This trend continues into November, when sensible heat fluxes nearly equal that of evaporation. The seasonal increase in sensible cooling is associated with a corresponding upward trend in the Bowen ratio (Table 2, Fig. 4d), similar to what has been found for Lake Mendota in southern Wisconsin (Stauffer, 1991). The two remaining terms in the energy budget (sediment heat flux and advection) have a net cooling effect on Sparkling Lake until around late September, when the value turns positive (Fig. 3). The magnitude (up to -6.5 W m^{-2}) is comparable to sensible cooling rates during the first two months of the season but otherwise is considerably weaker than other components of the energy budget.

Although the energy budget is a useful tool for calculating evaporation rates, its utility for understanding the climatic mechanisms controlling evaporation is somewhat limited (particularly for timescales less than a year). This is because, in the context of the energy budget, evaporation is a driver (of lake heat storage) as well as a response (to radiation, often with significant time lags). Arguably, a more fundamental driver of lake evaporation is the vapor pressure difference between water and air, which is strongly dependent on factors such as temperature, humidity, and wind speed. Fig. 4 illustrates a number of these climatic influences for Sparkling Lake, focusing on the average seasonal cycle (1989–1998 in most cases; Table 2).

The previously noted seasonal variations in evaporation are even more evident in Fig. 4a. Despite the conservative error estimates, autumn evaporation rates still fall well below those earlier in the year. The larger error bars in springtime are the result of larger net radiation, lower Bowen ratios, and more frequent

use of auxiliary radiation data. As a percentage of the mean, maximum evaporation errors typically range between 13 and 23% and are lowest in the middle of the season (July–September). For comparison, monthly mean evaporation estimates from Krabbenhoft et al. (1990b) are also shown in Fig. 4a (based on average pan evaporation rates for two lakes within 20 km of Sparkling Lake). The pan evaporation estimates, like the energy budget values, clearly show the distinct seasonality of lake evaporation in this region. The agreement between the two datasets is particularly good during July and August, but evaporation is significantly underestimated by the pan method during September and October (by 30–40%). As noted by Stauffer (1992), this discrepancy is due to the fact that the pan evaporation estimates of Krabbenhoft et al. (1990b) are based on lakes that are much shallower than Sparkling Lake and, therefore, have significantly less seasonal heat storage.

The distinct seasonal variation in Sparkling Lake evaporation rates (Fig. 4a) is largely explained by similar variations in lake surface temperature (Fig. 4b), which reaches its maximum during the same two-week period and is strongly correlated with evaporation (Table 3). Air temperature follows a similar curve (Fig. 4b) and is, on average, 2–6 °C cooler than the water surface (Fig. 4d). This temperature difference is greatest in autumn and is partly responsible for the previously noted changes in sensible heat flux and Bowen ratio (Table 2), which increases from around 0.1 in springtime to 0.85 by early November (Fig. 4d). Through the non-linear effect of temperature on vapor pressure, seasonal changes in water and air temperature lead to a vapor pressure difference curve that is very similar to that of the calculated evaporation rate (Fig. 4a and c, Table 3). Intraseasonal variations in lake–air temperature difference (Fig. 4d), such as the low values in mid June and late August, are also reflected in both the vapor pressure difference (Fig. 4c) and evaporation curves (Fig. 4a). This is encouraging, since it suggests that the simpler mass transfer method might provide adequate estimates of Sparkling Lake evaporation rates. The correspondence between evaporation and vapor pressure difference also helps to corroborate the results of the more rigorous energy budget method.

In addition to temperature, other meteorological factors likely to affect seasonal evaporation rates

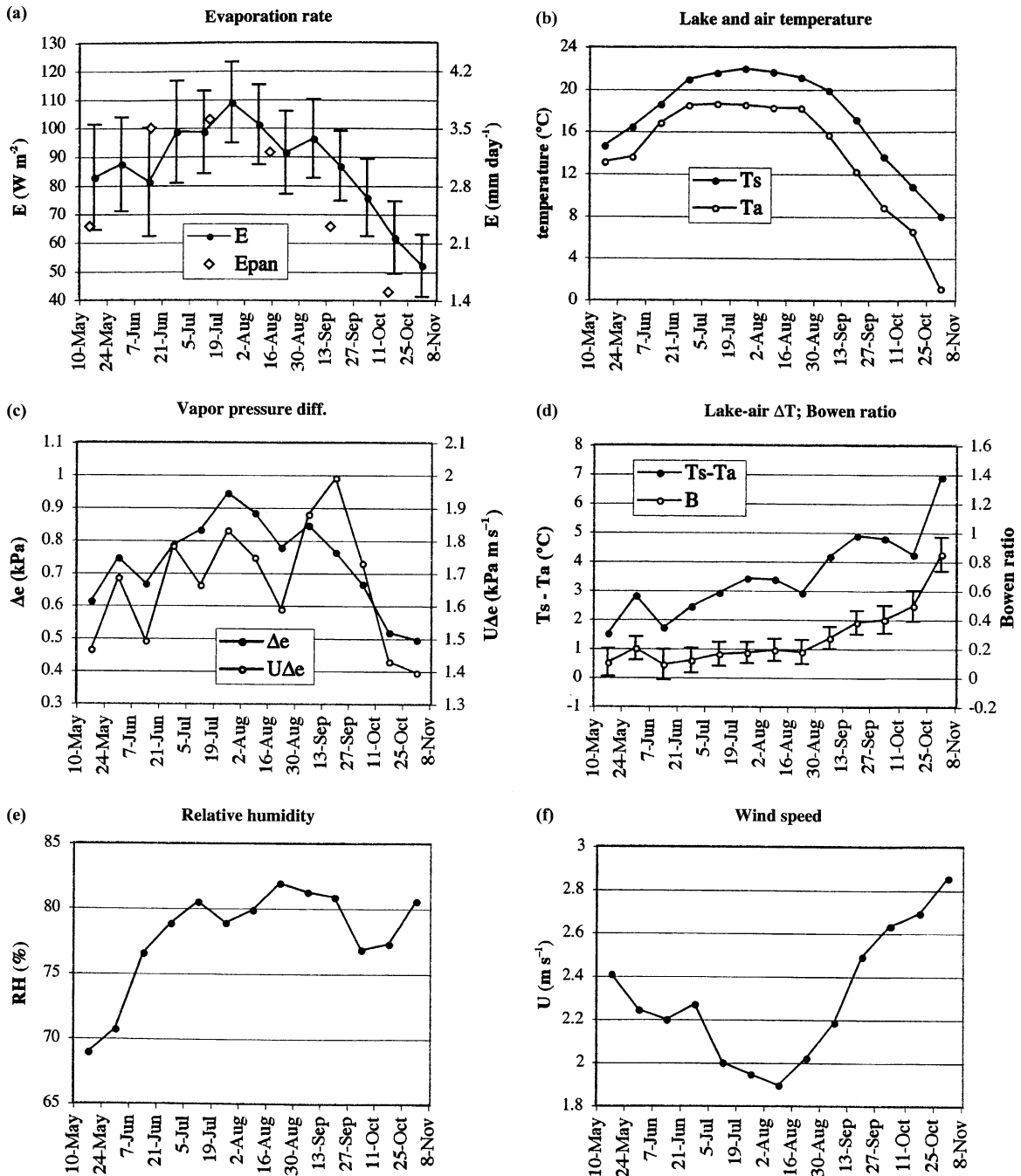


Fig. 4. Mean seasonal variability of atmospheric and limnological variables for Sparkling Lake (averaged over the number of years indicated in Table 2). Quantities include (a) evaporation rate in $W m^{-2}$ and $mm day^{-1}$ (E : energy budget; E_{pan} : average pan evaporation rate for two nearby lakes from Krabbenhoft et al., 1990b), (b) lake surface temperature (T_s ; $^{\circ}C$) and 2-m air temperature (T_a ; $^{\circ}C$), (c) lake-air vapor pressure difference (Δe ; kPa) and its product with wind speed ($U\Delta e$; $kPa m s^{-1}$), (d) lake-air temperature difference ($T_s - T_a$; $^{\circ}C$) and Bowen ratio (B ; unitless), (e) relative humidity (RH ; %), and (f) wind speed (U ; $m s^{-1}$). Error bars for E and B indicate the estimated maximum uncertainty.

Table 3

Correlation coefficients between Sparkling Lake evaporation rate and various energy budget and atmospheric quantities, as a function of timescale. Δe denotes the lake–air vapor pressure difference, and other variables are defined in Table 1. Correlations which are statistically significant at the 90% level are in italics, and insignificant values are bracketed. Seasonal correlation values have not been rigorously assessed for significance due to the large autocorrelation in the seasonal timeseries.

Timescale	R_{net}	S	H	B	T_s	T_a	$T_s - T_a$	RH	U	Δe	$U\Delta e$
Seasonal	0.78	0.61	−0.59	−0.79	0.96	0.93	−0.54	[0.15]	−0.90	0.96	0.68
Interannual	<i>0.91</i>	[0.12]	[−0.31]	−0.72	[0.11]	[0.38]	−0.78	[−0.49]	[0.18]	[0.38]	[0.36]
Intraseasonal	[0.17]	−0.63	0.55	[0.14]	[0.15]	−0.23	0.47	−0.57	0.40	0.68	0.70

include relative humidity and wind speed. Average variations in relative humidity over Sparkling Lake (Fig. 4e) show an increase from roughly 70% early in the season to around 80% by mid July. Although these seasonal changes are rather minor compared to temperature, they are large enough to produce noticeable differences in evaporation rate. For example, if the relative humidity during the first two-week period was increased from the observed value (69%) to a mid-season value (80%), the water–air vapor pressure difference would be reduced by 28%. This suggests that relative humidity variations (Fig. 4e) moderate the temperature-induced seasonality in evaporation by raising evaporation rates during the springtime and lowering them during the summer and fall. A caveat here is that estimated maximum errors in relative humidity (Table 1) are similar in magnitude to the observed seasonal variability. However, relative humidity data for Antigo, Wisconsin (not shown) reveal similar seasonal variability, suggesting that the pattern is robust.

Average wind speeds over Sparkling Lake (Fig. 4f) show a pattern of low wind speeds during July and August and relatively higher values during spring and (especially) autumn. This is likely to be due to the fact that extratropical cyclones in this region tend to be more frequent and intense during the spring and fall than during the summer (Angel and Isard, 1998). Note that this seasonal wind pattern (Fig. 4f) is roughly out-of-phase (Table 3) with the evaporation curve (Fig. 4a). As a result, inclusion of wind speed as a linear term in the vapor pressure difference curve (Fig. 4c) leads to a less favorable comparison with the energy budget-derived evaporation rates (Fig. 4a; Table 3). This unexpected result suggests that, on seasonal timescales, it may not be appropriate to include wind speed as a linear term in mass transfer

evaporation estimates for Sparkling Lake (or other lakes with similar seasonal variations in climate). A possible explanation for this is that the lower boundary layer may be sufficiently well mixed for wind speeds of 2–3 m s^{−1}, such that the small seasonal variations (Fig. 4f) have little, if any impact on evaporation.

4.3. Interannual variability

As noted earlier in Fig. 2, Sparkling Lake experiences significant interannual variations in evaporation. This is also evident in the interannual coefficient of variation (c.v.) in evaporation for each of the 13 energy budget periods (not shown). Typical year-to-year variations in 14-day mean evaporation range from 15 to 25% of the average evaporation rate and are usually larger than the maximum error bounds. A prominent exception to this is the period 21 June–5 July, when evaporation rates are remarkably consistent, year to year (c.v.=8%). This may indicate a particularly quiescent time of year for the local climate (similar to what was found for Perch Lake by Robertson and Barry, 1985), although large error bars prevent a conclusive determination at this point. Relatively large interannual variability occurs during 10–24 May (c.v.=37%). Although this reflects only 2 years of data (Table 2), it is consistent with the results of Robertson and Barry (1985), who found year-to-year changes in evaporation to be highest during the month of May (c.v.=24%). For comparison, Winter et al. (2003) found monthly mean evaporation rates for Mirror Lake to be most variable (from year to year) for October (c.v.=32%) and least variable for September (c.v.=6%). Other months generally had an interannual coefficient of variation of around 12–16% (Winter et al., 2003).

Table 4

Interannual variability in the Sparkling Lake energy budget. Quantities are averaged over the 14-week summer period (italicized in Table 2) for each of the 10 years. Also shown are the long-term mean and interannual standard deviation. Variables are defined in Table 1.

Year	<i>E</i> (mm day ⁻¹)	<i>E</i> (W m ⁻²)	<i>R</i> _{net} (W m ⁻²)	<i>S</i> (W m ⁻²)	<i>H</i> (W m ⁻²)	<i>B</i>
1989	4.11	117.0	144.2	4.3	18.2	0.16
1990	3.72	106.0	131.5	2.6	18.5	0.17
1991	3.79	108.1	125.7	-9.5	22.5	0.21
1992	3.15	89.7	112.2	2.2	16.2	0.18
1993	3.43	97.7	117.9	0.3	15.6	0.16
1994	2.79	79.6	101.1	-4.7	22.2	0.29
1995	3.24	92.4	110.8	-11.5	25.4	0.27
1996	3.25	92.4	124.2	4.3	23.1	0.26
1997	3.09	88.0	119.8	6.7	20.9	0.24
1998	3.61	102.8	129.6	6.4	15.9	0.16
Mean	3.42	97.4	121.7	0.1	19.9	0.21
SD	0.39	11.1	12.2	6.5	3.5	0.05

To assess interannual variations in summer averages (rather than 14-day periods), 14-week means were created for each year by averaging the energy budget and meteorological variables over seven energy budget periods from 21 June to 27 September (the italicized periods in Table 2). The first and last three energy budget periods (Table 2) were excluded from the averaging process because data were not available for the full 10 years during the spring and late autumn. Average energy budget components for each year are shown in Table 4 along with the 10-year means and standard deviations. Interannual variations in summertime net radiation, lake heat storage, sensible cooling, and Bowen ratio (Table 4) are considerably smaller than corresponding seasonal variations (Table 2). This is primarily because seasonal variations in temperature and solar radiation are significantly larger than year-to-year variations (particularly when averaged over a 14-week period). The interannual standard deviation of evaporation rate (Table 4) is also less than that of the seasonal cycle (Table 2), but only by a small amount. In fact, year-to-year variations in *E*, *R*_{net}, *H*, and *B* are roughly 11, 10, 18, and 24% of their mean values, respectively. This indicates that interannual changes in the energy budget, though smaller than seasonal variations, are not insignificant. Results from Winter et al. (2003) and Sturrock et al. (1992) show similar interannual variations in summer evaporation for Mirror Lake (6-year c.v. = 9%) and Williams Lake

(5-year c.v. = 10%), respectively. Similarly, Robertson and Barry (1985) report a 10-year coefficient of variation of 8% for annual mean evaporation from Perch Lake. Even greater year-to-year changes in evaporation have been reported for some arctic lakes (Gibson, 2002).

To better understand the mechanisms and uncertainties associated with the interannual variations, energy budget anomalies were calculated. The anomalies represent deviations from the 10-year mean (Table 4) and are plotted, together with error bars, in Fig. 5. A significant, 32% drop in evaporation rate is evident from 1989 to 1994, followed by a rebound to higher evaporation in 1998 (Fig. 5a). Despite the relatively large error bars, 1994 evaporation rates are unquestionably lower than both 1989 and 1998. Other significant years include 1992 and 1997, when evaporation rates were notably lower than in 1989. Remaining year-to-year variations are less conclusive, since they fall within the estimated measurement uncertainty. Net radiation follows a similar pattern of interannual variability (Fig. 5b), including high net radiation during 1989 and 1998 and low values during 1992 and 1994. Most of this variability is associated with changes in incoming solar radiation, not longwave radiation (Fig. 5b). As shown in previous studies (e.g. Winter et al., 2003), the close correspondence between net radiation and evaporation rates (Fig. 5a and b, Table 3) indicates that, on these longer interannual timescales, radiation

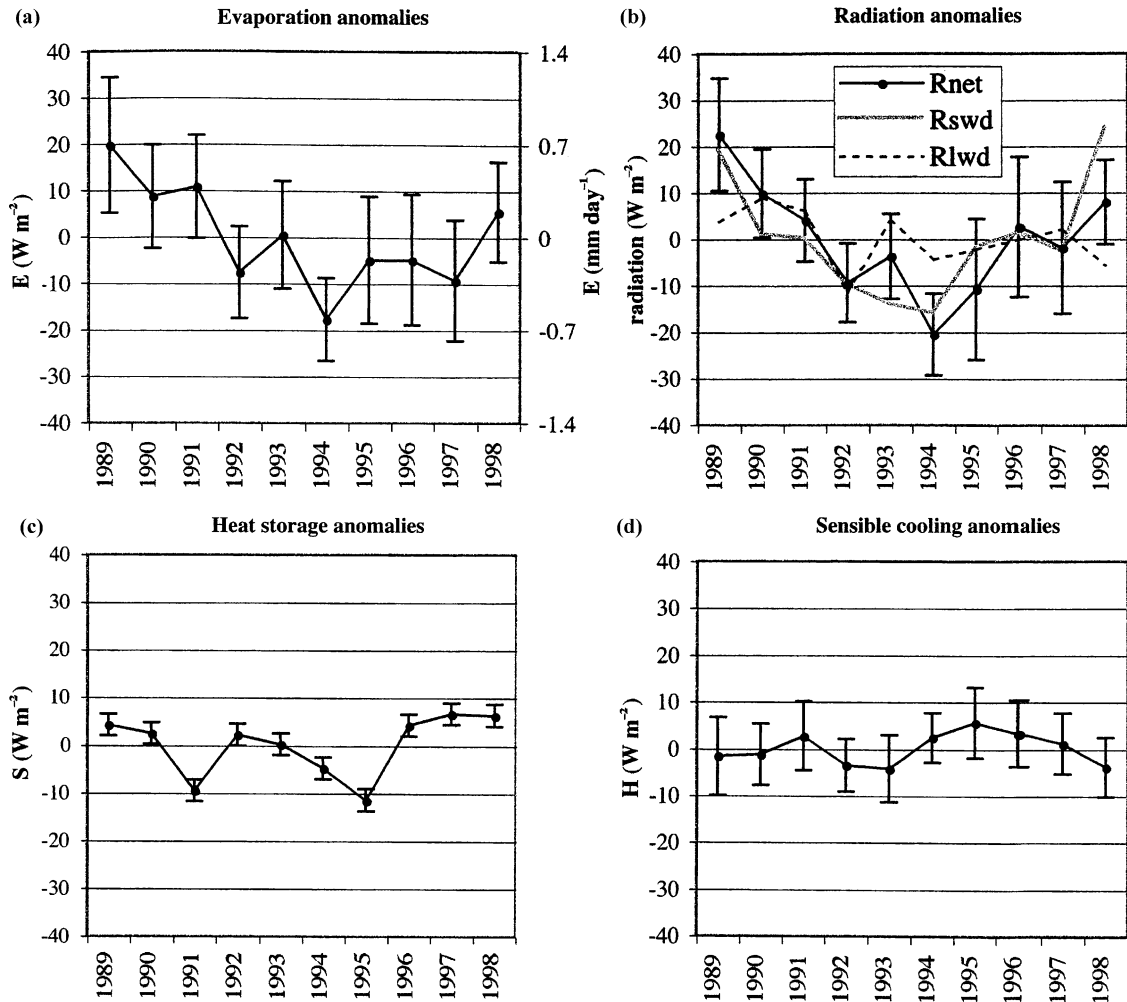


Fig. 5. Interannual variations in the summertime energy budget of Sparkling Lake for 1989–1998. Quantities are averaged over the 98-day period of June 21–September 27 and are expressed as anomalies (deviations from the 10-year mean). Energy budget components include (a) evaporation rate (E), (b) net radiation (R_{net}), downward shortwave radiation (R_{swd}), downward longwave radiation (R_{lwd}), (c) heat storage rate (S), and (d) sensible cooling rate (H). Units are in W m^{-2} (and mm day^{-1} for E), and error bars indicate the estimated maximum uncertainty (not shown for R_{swd} and R_{lwd}).

is an important driver of evaporation (since lake temperatures have sufficient time to adjust to changes in radiation). This is supported by the relatively small year-to-year changes in thermal storage (Fig. 5c). Sparkling Lake does, however, show anomalous losses of heat during 1991 and 1995 as a result of larger increases in evaporation (Fig. 5a) than radiation (Fig. 5b). This implies that meteorological factors other than radiation are playing a role as well. Finally, it is noted that sensible cooling anomalies (Fig. 5d)

show moderate interannual variability (compared to the mean), but with relatively high uncertainty.

As with the seasonal variability, we now examine other climatic variables related to the interannual changes in lake evaporation. These are shown in Fig. 6 as mean quantities (rather than anomalies). A comparison of Fig. 6a–c with the anomalous evaporation rates (Fig. 5a) reveals that neither surface temperature, relative humidity, nor wind speed are (by themselves) strongly related to changes in evaporation

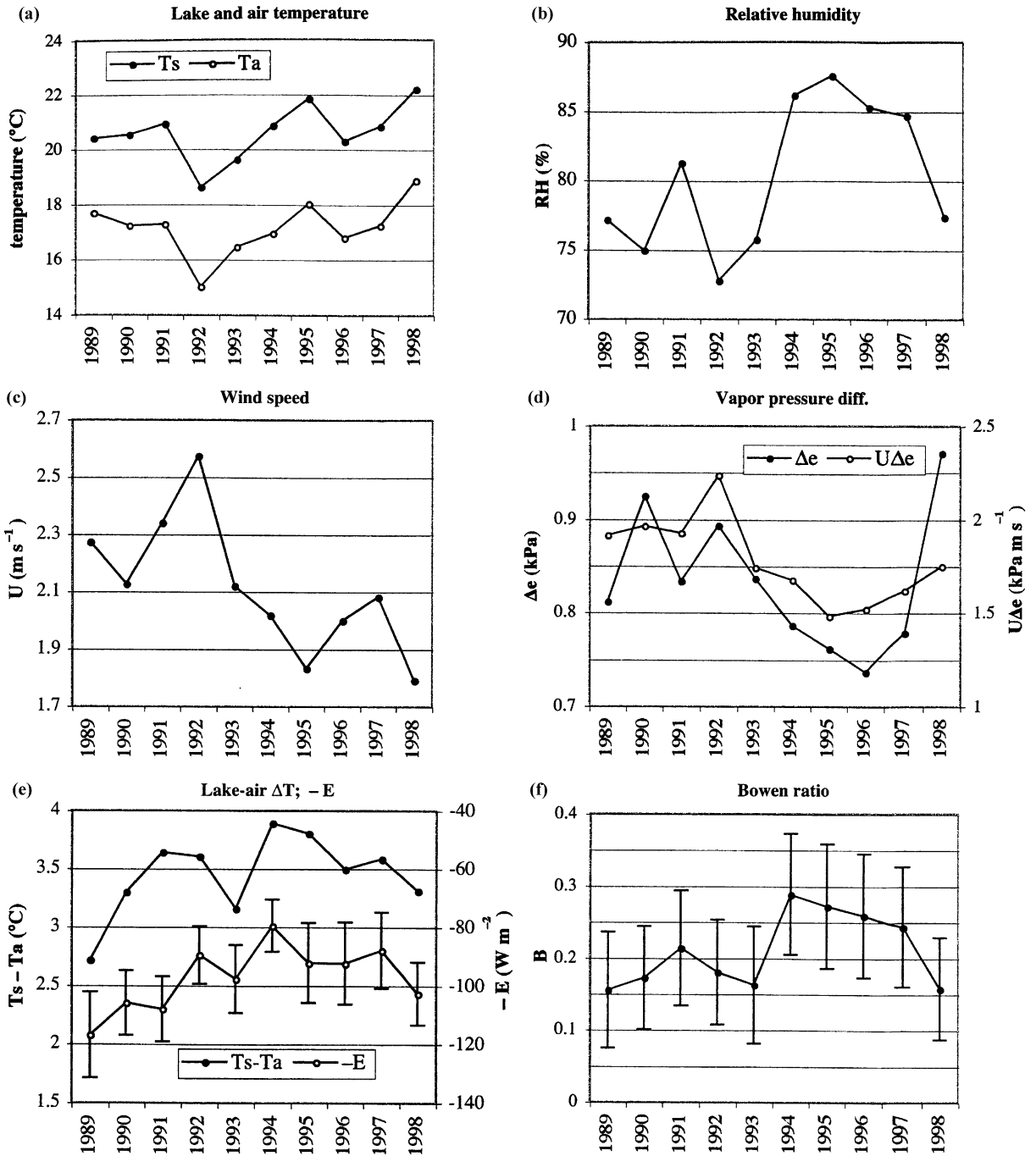


Fig. 6. Interannual variability of atmospheric and limnological variables for Sparkling Lake during 1989–1998 (averaged over the summer period of June 21–September 27). Quantities include (a) lake surface temperature (T_s ; °C) and 2-m air temperature (T_a ; °C), (b) relative humidity (RH; %), (c) wind speed (U ; $m\ s^{-1}$), (d) lake–air vapor pressure difference (Δe ; kPa) and its product with wind speed ($U\Delta e$; $kPa\ m\ s^{-1}$), (e) lake–air temperature difference ($T_s - T_a$; °C) and evaporative cooling rate ($W\ m^{-2}$; expressed as a negative quantity, $-E$), and (f) Bowen ratio (B ; unitless). Error bars for $-E$ and B indicate the estimated maximum uncertainty.

on interannual timescales (Table 3). Some correspondence, however, is evident. For example, the decrease in evaporation from 1991 to 1992 (Fig. 5a) is associated with the largest one-year drop in water and air temperatures during the 10-year period (Fig. 6a). (Interestingly, the relatively cool summer of 1992 was prevalent throughout North America and has been directly associated with the eruption of Mt Pinatubo during the previous year; Robock and Mao, 1995; Robock, 2002.) Similarly, a rebound to higher evaporation rates occurred in 1998, the warmest of the 10 years. This suggests that interannual changes in air temperature (through direct effects on water temperature) are driving some of the observed changes in evaporation. Relative humidity (Fig. 6b) shows a significant increase from 1992 to 1995 and is negatively correlated with evaporation (albeit weakly; Table 3). This suggests that high relative humidity from 1994 to 1997 may have contributed to below-normal lake evaporation during these years (Fig. 5a). In addition, wind speed exhibits an overall downward trend from 1989 to 1998 (Fig. 6c) in the order of -0.5 m s^{-1} over the 10-year period ($R^2=0.46$). This 22% drop in wind speed may be contributing to the observed downward trend in evaporation (Fig. 5a). Curiously, however, wind speed shows little year-to-year correspondence with anomalous evaporation rates (Figs. 6c and 5a; Table 3), similar to what was found for the seasonal variations.

When the effects of surface temperature and relative humidity are combined to form the interannual vapor pressure difference curve (Fig. 6d), one finds relatively few similarities with the evaporation anomalies (Fig. 5a), aside from the overall downward trend in evaporation from 1989 to 1994. Only 14% of the year-to-year changes in evaporation are explained by variations in lake–air vapor pressure gradient (Table 3), and no improvement is found when the effects of wind speed are included (aside from contributing to the downward trend). Since the mass transfer formulation ($U\Delta e$) is highly sensitive to errors in temperature, relative humidity, and wind speed (more so than the energy budget technique; Winter, 1981), it is entirely possible that the uncertainties in T_s , T_a , RH, and U (Table 1) are simply too large (relative to the actual interannual variability) to justify using the mass transfer technique to calculate interannual changes in evaporation.

This was not an issue with the seasonal changes in evaporation because, in that case, the vapor pressure curve is dominated by much larger changes in surface temperature (Fig. 4b–c).

Two parameters which do show a close relationship with interannual changes in evaporation are the lake–air surface temperature difference (Fig. 6e) and, correspondingly, the Bowen ratio (Fig. 6f). The error bars are somewhat large for the Bowen ratio, so we focus our discussion on the temperature variations, which are likely to be more robust. Interannual changes in lake–air temperature difference (Fig. 6e) are negatively correlated with evaporation (Fig. 5a) and explain 60% of the variance (Table 3). (A plot of $-E$ is also shown in Fig. 6e to better illustrate the correspondence between the two curves.) Initially, this result seemed rather surprising, since temperature effects on lake–air vapor pressure difference would suggest a positive correlation (as was found in Fig. 4a–d for some intraseasonal changes in evaporation). However, an important consideration of the longer, interannual timescale is that lake surface temperature has ample time to adjust to changes in surface heat flux. This leads, for example, to highly coherent variations in air and water temperature ($R^2=0.89$, Fig. 6a; see also Livingstone and Dokulil, 2001) and, correspondingly, relatively subtle variations in lake–air temperature difference ($SD=0.3 \text{ }^\circ\text{C}$, Fig. 6e). These small temperature changes make it difficult to try and explain the relationship between E and $T_s - T_a$ in terms of vapor pressure differences, particularly since the influence of relative humidity can significantly mask the temperature effects. If, instead, one adopts an energy budget perspective (where evaporative heat flux drives changes in temperature), a potential explanation for the correlation in Fig. 6e arises. Specifically, although evaporation generally increases with increasing temperature (larger vapor pressure difference), the negative feedback of evaporative cooling limits the temperature increase of the water. Thus, an increase in air temperature (and, presumably, net radiation) is associated with a lesser increase in lake temperature (because of higher evaporation), leading to a smaller lake–air temperature difference; hence, the negative relationship between evaporation (Fig. 5a) and $T_s - T_a$ (Fig. 6e). The same can be said for humidity or wind speed-driven changes in evaporation, since long-term

increases in evaporation eventually lead to decreases in lake surface temperature if there is no compensatory change in air temperature (or radiation). In fact, just such a situation is evident in a 7-year simulation of lake evaporation for Harney–Malheur Lake in Oregon (Hostetler and Bartlein, 1990). During the last three years of the simulation, modeled summer evaporation progressively increased in response to higher wind speeds and lower vapor pressure (Hostetler and Bartlein, 1990). Although not commented on specifically, it is evident that the modeled water surface temperature also decreased over the same time period, while air temperature remained relatively unchanged. This indicates a decrease in lake–air temperature difference in conjunction with increased evaporation rates (i.e. consistent with the pattern in Fig. 6e). Similarly, lower evaporation rates would be associated with a higher lake–air temperature difference. These results suggest that it may be possible to use the lake–air temperature difference as a diagnostic indicator of long-term variations in evaporation rate.

The moderating effect of evaporative cooling on increases in water temperature (particularly at high temperatures) is not a new idea and has been noted in previous studies (e.g. Hondzo and Stefan, 1993; Mohseni and Stefan, 1999; Peeters et al., 2002). To the authors’ knowledge, however, observational evidence that this water/air temperature relationship

can be exploited as a simple method for estimating interannual variations in lake evaporation has not been previously reported. This is likely due to the limited number of long-term studies of lake evaporation as well as the more prevalent use of the mass transfer technique. But since the mass transfer relationship appears to perform poorly on interannual timescales (in this study and others, such as Sturrock et al., 1992; Sacks et al., 1994), we instead develop an alternative empirical relationship. Fig. 7 shows a scatter plot of mean evaporation (21 June–27 September) vs. lake–air temperature difference (each dot representing a year). Linear regression yields the following relationship

$$\langle E \rangle = C_1(T_s - T_a) + C_2, \tag{14}$$

where $C_1 = -25.15 \text{ W m}^{-2} \text{ }^\circ\text{C}^{-1}$ ($0.883 \text{ mm day}^{-1} \text{ }^\circ\text{C}^{-1}$), $C_2 = 184.15 \text{ W m}^{-2}$ (6.47 mm day^{-1}), and the brackets indicate a 14-week summer mean. The linear fit is found to approximate evaporation quite well ($R^2 = 0.60$) and falls within the error bounds for 9 of the 10 years (1991 being the exception). We caution that the regression coefficients, C_1 and C_2 (like similar coefficients, such as those used in the mass transfer technique), are likely to be dependent on individual lake characteristics as well as factors such as local climate and averaging period. Thus, a relationship such as Eq. (14) cannot necessarily be expected to apply for other lakes, regions, or times of

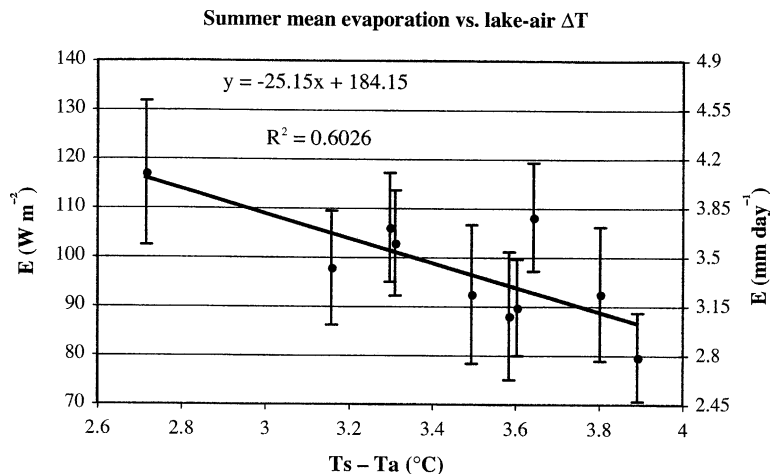


Fig. 7. Summer mean evaporation rate for Sparkling Lake (E , in W m^{-2} and mm day^{-1}) vs. lake–air temperature difference ($T_s - T_a$; $^\circ\text{C}$). Each dot represents one year (during 1989–1998), averaged over the 98-day period June 21–September 27. Error bars indicate the estimated maximum uncertainty in evaporation rate. Also shown are the linear regression line and its associated equation (in W m^{-2}) and R^2 value.

the year. Eq. (14) does, however, provide a useful approximation of the summertime evaporation rates for Sparkling Lake during 1989–1998. Eventual analyses for 1999 and beyond will allow us to assess the long-term validity of this relationship.

4.4. Short-term variations

To analyze the short-term, intraseasonal variations in evaporation rate, anomalies are calculated for each 14-day period. This is done by first removing the average seasonal cycle (Fig. 4a) from the raw timeseries (Fig. 2, sampled every 14 days). Next, interannual variations are removed by subtracting the annual anomalies (Fig. 5a). The same procedure is then used to calculate intraseasonal anomalies for other energy budget and climatic variables. Since the interannual variations are based on the period 21 June–27 September, we restrict our analysis of the short-term variability to this same 14-week period. Although this eliminates consideration of some intraseasonal variations during the spring and fall (Table 2), it allows us to be confident that robust seasonal and interannual variations have largely been removed (since all 10 years of data are utilized). With seven energy budget periods for each year, this leads to a total of 70 samples for examining short-term variations in evaporation rate.

The standard deviation of intraseasonal evaporation anomalies is 13.7 W m^{-2} , which is smaller than the seasonal variability (Table 2) but larger than the interannual standard deviation (Table 4). Net radiation anomalies are rather normally distributed about zero (not shown) with a standard deviation of 15.2 W m^{-2} (slightly larger than the interannual variability; Table 4). Anomalous heat storage shows a much larger standard deviation (24.5 W m^{-2}) since it combines the influences of both radiative and surface heat fluxes. This value is considerably larger than the interannual variability (Table 4), but still less than the seasonal standard deviation (Table 2). Sensible cooling exhibits a relatively small standard deviation (7.4 W m^{-2}) compared to intraseasonal variations in the other energy budget components. Nevertheless, this amount of variability is roughly twice the interannual value (Table 4). Bowen ratio anomalies are normally distributed with a standard deviation of 0.06 (comparable to the interannual variability).

The covariances of various energy budget components are illustrated in Fig. 8. Similar to the results of Blanken et al. (2000), net radiation and evaporation are essentially uncorrelated (Fig. 8a), indicating that short-term variations in Sparkling Lake evaporation are not driven by radiation anomalies during the same 14-day period. (Possible lag relationships are investigated later.) Evaporation is negatively correlated with lake heat storage (Fig. 8b) and, therefore, is an important driver of intraseasonal lake temperature changes. Since evaporation and sensible cooling anomalies are moderately correlated (Fig. 8c), changes in either component typically result in even larger changes in lake heat storage (Fig. 8b and d). The correlation is strongest for sensible cooling (Fig. 8d; $r = -0.85$), since both lake heat storage and sensible heat flux are primarily functions of temperature. (Evaporative heat flux is complicated by the effects of humidity and exhibits significantly more variability.) It is also worth noting that intraseasonal variations in Bowen ratio show essentially no relationship to changes in evaporation (Table 3).

Connections between short-term variations in evaporation and local climate are examined in Fig. 9. Lake temperature anomalies are not significantly related to intraseasonal changes in evaporation (Fig. 9a). This is primarily because lake temperature increases are usually accompanied by higher air temperatures as well ($R^2 = 0.53$), which reduces the vapor pressure deficit. In fact, the effects of air temperature on absolute humidity outweigh the impact on lake temperature, resulting in a slightly negative (and statistically significant) relationship between air temperature and evaporation (Fig. 9b; Table 3). Combined with the effects of water temperature, this leads to a relatively strong correlation between evaporation and the lake–air temperature difference (Fig. 9c; Table 3). Unlike the interannual variations, the correlation is positive. This implies that, on 14-day timescales, vapor pressure effects on evaporation dominate the negative feedback of evaporative cooling. It is also possible (as noted by Assouline and Mahrer, 1993) that the connection between evaporation and lake–air temperature difference is due, in part, to the effects of atmospheric stability (i.e. higher $T_s - T_a$, greater instability, higher evaporation).

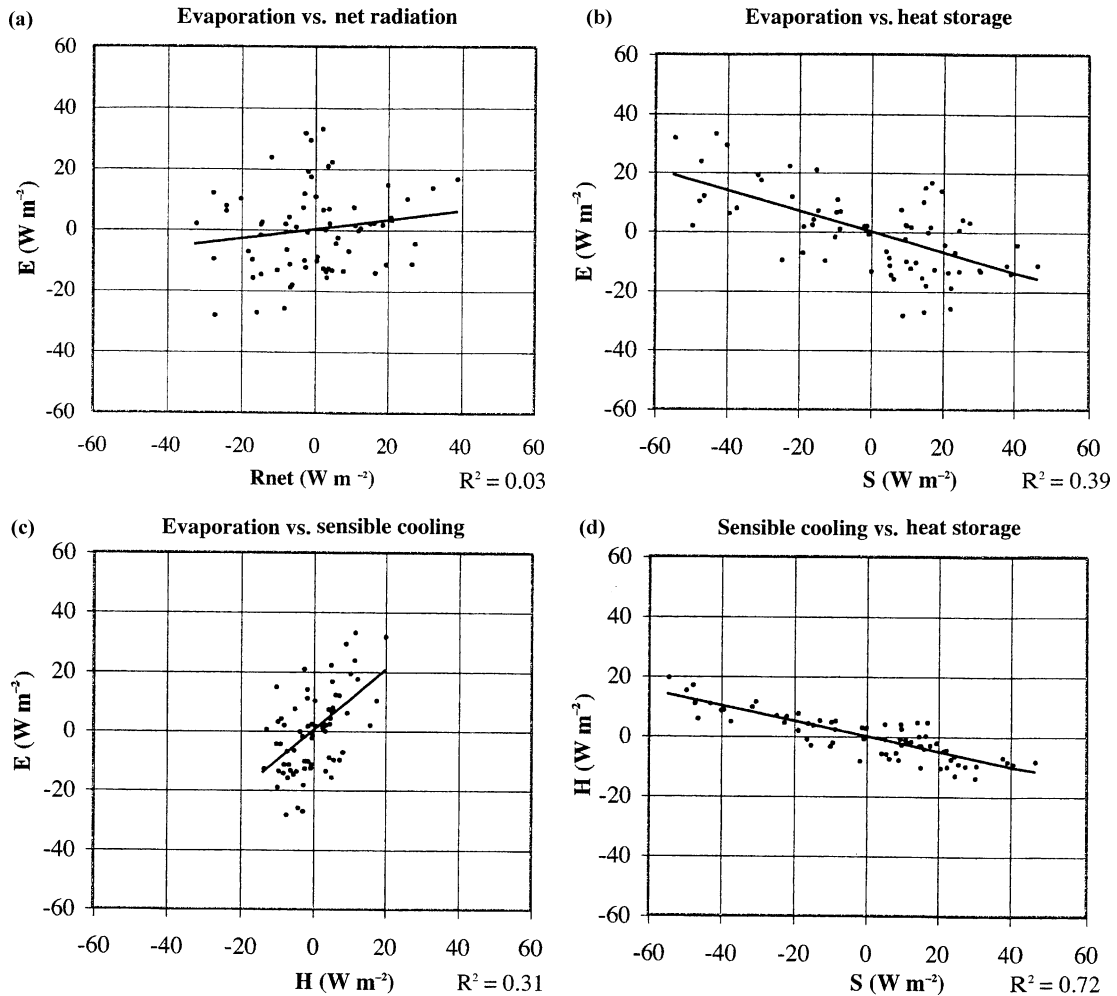


Fig. 8. Sparkling Lake evaporation rate (E) vs. (a) net radiation (R_{net}), (b) heat storage rate (S), and (c) sensible cooling rate (H). (d) Sensible cooling rate (H) vs. heat storage rate (S). All quantities are in W m^{-2} and are expressed as intraseasonal anomalies (14-day deviations from the mean seasonal and interannual variability). Each dot represents one of 70 bi-weekly periods during the 10 summers (June 21–September 27, 1989–1998). Also shown are the linear regression lines and associated R^2 values.

Relative humidity exhibits a significant, negative correlation with intraseasonal evaporation anomalies (Fig. 9d, Table 3). This is physically intuitive and lends some confidence to the otherwise uncertain relative humidity measurements. When temperature and humidity are combined into vapor pressure anomalies, the resulting relationship with evaporation is strongly positive (Fig. 9e, Table 3). This verifies the vapor pressure connection first seen in Fig. 4a and c and indicates that a mass transfer approximation is suitable for intraseasonal timescales (as it is also for seasonal timescales, but not interannual). In contrast

to the seasonal and interannual timescales, short-term variations in wind speed are moderately correlated with evaporation (Fig. 9f), as was also found by Blanken et al. (2000) for Great Slave Lake. However, including it with vapor pressure in the mass transfer formula ($U\Delta e$, Table 3) leads to little improvement in the overall relationship (from $R^2=0.46$ to 0.48).

To better illustrate the temporal relationship between temperature and evaporation on intraseasonal timescales, Fig. 10 shows examples of various timeseries for 1994. This includes 14-day running mean anomalies of E , T_s , T_a , and $T_s - T_a$.

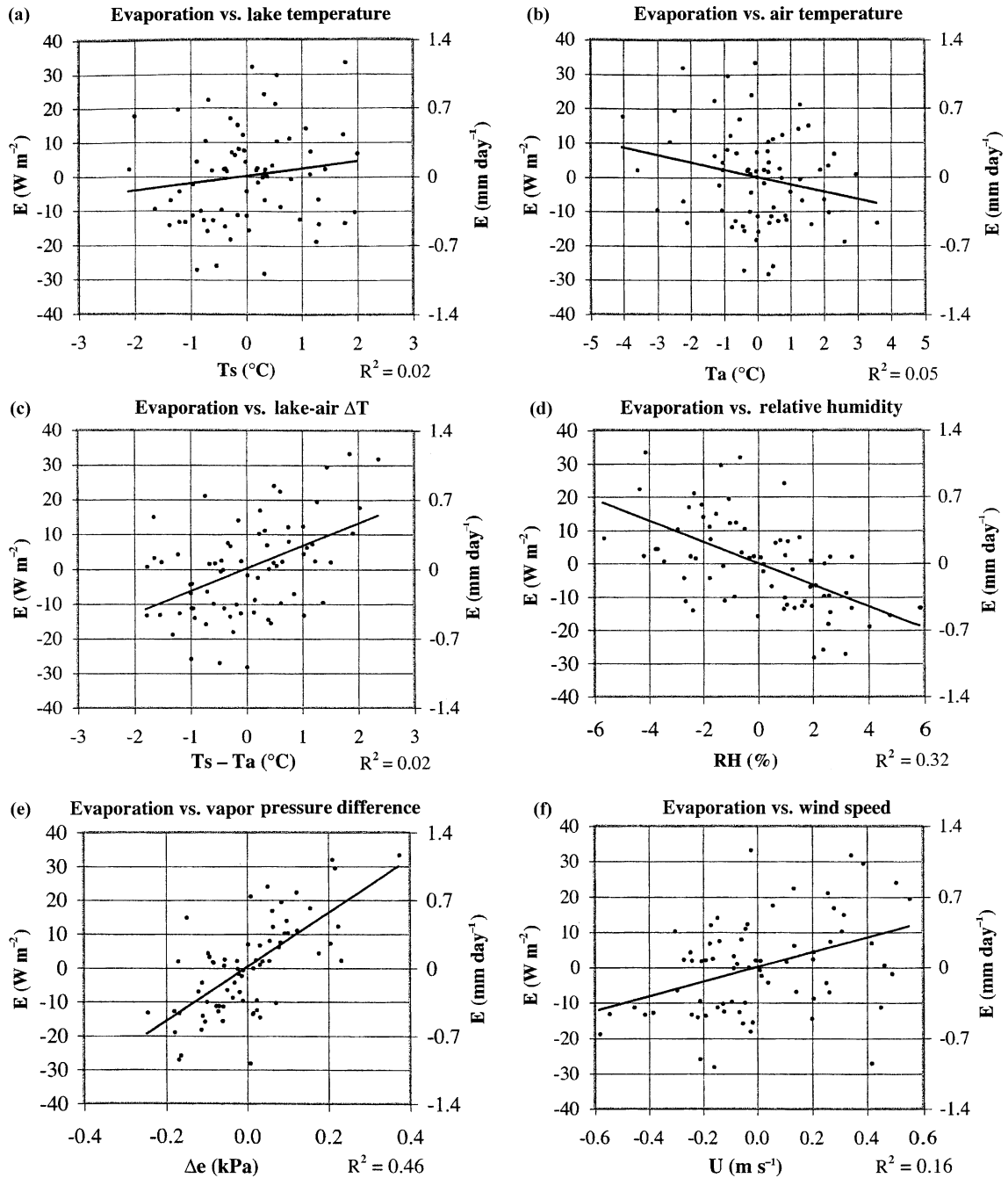


Fig. 9. Sparkling Lake evaporation rate (E , in W m^{-2} and mm day^{-1}) vs. (a) lake surface temperature (T_s ; $^{\circ}\text{C}$), (b) 2-m air temperature (T_a ; $^{\circ}\text{C}$) (c) lake–air temperature difference ($T_s - T_a$; $^{\circ}\text{C}$), (d) relative humidity (RH; %), (e) lake–air vapor pressure difference (Δe ; kPa), and (f) wind speed (U ; m s^{-1}). All quantities are expressed as intraseasonal anomalies (14-day deviations from the mean seasonal and interannual variability). Each dot represents one of 70 bi-weekly periods during the 10 summers (June 21–September 27, 1989–1998). Also shown are the linear regression lines and associated R^2 values.

Predominant seasonal and interannual variations have been subtracted (as before), but the data are now presented on a daily basis (rather than sub-sampled every 14 days) in order to more clearly illustrate the temporal evolution. Evaporation shows a series of three well-defined peaks (beginning around August 9) surrounded by four corresponding troughs. The variability is quasi-periodic over a timescale of roughly 20–40 days and is distinctly phase-shifted from the air and water temperature variations (Fig. 10). In particular, variations in 14-day mean air temperature precede similar (but damped) variations in water temperature by roughly 3–5 days, due to the thermal inertia of the lake (Edinger et al., 1968). Water temperature, in turn, leads evaporation by another 5–10 days (because of the competing influence of air temperature on the vapor pressure difference and atmospheric stability). This leads to an overall 8–15-day lag between air temperature and evaporation and, therefore, an approximately out-of-phase relationship between the two curves (Fig. 10; Table 3). If, however, one combines the time lags of air and water temperature into a difference curve ($T_s - T_a$), then a strong, positive relationship with evaporation emerges (Fig. 10). As noted above, this proxy for vapor pressure difference is significantly correlated with evaporation on intraseasonal timescales (Table 3).

Although the previous example focused on the year 1994, the general conclusions regarding time lags are found to hold over the 10-year period as a whole. This was verified by calculating the lag correlation coefficient between 14-day running mean anomalies of evaporation and T_s , T_a , $T_s - T_a$, and R_{net} (not shown; based on all available data during the 10 years). The strongest correlation between air temperature and evaporation ($r=0.50$) occurs at a time lag of -12 days (temperature leading evaporation). This is followed in time by water temperature, which leads evaporation by 5–8 days ($r=0.53$), and $T_s - T_a$, which is roughly coincident with evaporation ($r=0.40$ at lag-0). There is also a tendency for evaporation anomalies to be preceded by $T_s - T_a$ anomalies (of the opposite sign) 15 days earlier ($r=-0.37$). Based on Fig. 10, this behavior appears to be due to the episodic nature of the local climate and the associated periodicity in evaporation and $T_s - T_a$. This has been verified by plotting the autocorrelation function for E and $T_s - T_a$ (not shown). Such a plot indicates that (for both variables) positive anomalies tend to be preceded by negative anomalies 15–20 days in advance (yielding a periodicity of roughly 30–40 days). Finally, we note that net radiation is significantly correlated with evaporation when leading the latter by 7–11 days ($r=0.42$). Thus, although high radiation

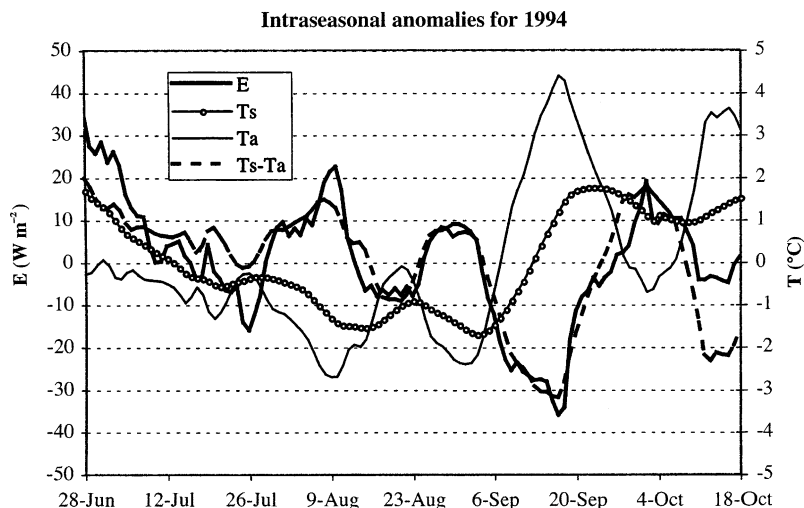


Fig. 10. Intraseasonal variations in evaporation rate (E , in W m^{-2}) for Sparkling Lake during the summer of 1994. Also shown are the lake surface temperature (T_s), 2-m air temperature (T_a), and lake–air temperature difference ($T_s - T_a$) in units of $^{\circ}\text{C}$. All quantities are calculated as centered, 14-day running mean anomalies (deviations from the mean seasonal and interannual variability).

does not generally result in increased evaporation during the same 14-day period (Table 3), subsequent heating of the lake (perhaps accompanied by reduced air temperature and humidity) leads to higher evaporation rates within the next week or two.

5. Summary and conclusions

This study has provided a comprehensive 10-year analysis of seasonal, intraseasonal, and interannual variations in lake evaporation using the energy budget method. Special care has been taken to provide error estimates so that real variations in evaporation (and other energy budget quantities) can be adequately assessed. The long-term mean evaporation rate for Sparkling Lake is found to be 3.1 mm day^{-1} (averaged over all available 14-day periods), with a standard deviation of 0.8 mm day^{-1} . The estimated maximum error bounds for evaporation typically range from 10 to 22% of the 14-day mean evaporation (10–14% for summer-long averages). Since these are maximum bounds, actual errors are more likely to be in the range of 5–10% (except during periods which utilize auxiliary radiation data).

Our conclusions are based on data from Sparkling Lake, Wisconsin, but are likely to be valid for most mid-latitude lakes of comparable size. First and foremost, we find that lake evaporation is highly variable on a wide range of timescales. This is particularly true for the seasonal timescale, which exhibits an average range in evaporation from 2.9 mm day^{-1} in late May to 3.8 mm day^{-1} in late July to 1.8 mm day^{-1} in early November. These values are comparable to the long-term monthly mean evaporation rates for Perch Lake (Robertson and Barry, 1985), Williams Lake (Sturrock et al., 1992), and Mirror Lake (Winter et al., 2003) and closely follow the seasonal changes in Sparkling Lake surface temperature (from 15°C in late May to 22°C in late July to 8°C in early November). Net radiation also shows similar behavior, but precedes the temperature and evaporation maxima by roughly one month. Low relative humidity in late spring moderates the seasonal variation in evaporation somewhat, while wind speed variations are distinctly out-of-phase with those of evaporation. This is a somewhat unexpected result, but simply indicates the tendency for higher wind

speeds in spring and (especially) autumn, when extratropical storms tend to be more frequent and intense (Angel and Isard, 1998).

Even though the seasonal cycle is clearly evident when evaporation rates are averaged over all available years, it is much more poorly defined for individual years because of significant intraseasonal variations. The standard deviation of intraseasonal lake evaporation (14-day means with seasonal and interannual variations removed) is roughly 86% of the seasonal standard deviation and more than 15% of the long-term mean evaporation rate. These large within-season variations are the result of frequent (and somewhat regular) synoptic weather variations which influence the region on 14- to 30-day timescales. The most important individual climatic influence on intraseasonal variations in evaporation is relative humidity, which explains 32% of the variance in lake evaporation. This is followed by lake–air temperature difference ($R^2=0.22$), wind speed ($R^2=0.16$), and air temperature ($R^2=0.05$), which is negatively correlated with evaporation (largely because of the influence of air temperature on atmospheric humidity). Combining the effects of temperature and humidity, it is found that vapor pressure difference explains roughly 46% of the variance in intraseasonal evaporation rates (with little improvement by including wind speed). Neither water temperature nor net radiation show a significant relationship with evaporation on intraseasonal timescales, except when leading evaporation changes by 5–11 days. These time lags result from the thermal inertia of the lake as well as the competing effects of atmospheric humidity. For example, 14-day periods of warm weather are generally coincident with low, rather than high evaporation rates for Sparkling Lake because of the correspondingly high levels of atmospheric humidity. It is not until a week or two later, when water temperature has increased (in response to the previously warm conditions) and air temperature and humidity have dropped (in association with typical synoptic variability, such as a frontal passage) that evaporation rates reach high levels. This difference in timing between water and air temperatures (which is largely a function of lake depth and regional climatic variability) is critical to understanding intraseasonal variations in lake evaporation.

Year-to-year changes in mean summer evaporation (21 June–27 September), while generally smaller than the seasonal and intraseasonal variations, are by no means negligible. The interannual standard deviation of 14-week evaporation is roughly 70% of the seasonal value and more than 11% of the long-term mean evaporation rate. These interannual variations are largely driven by changes in net radiation ($R^2=0.83$), particularly shortwave radiation (through variations in cloud cover, aerosols, etc.). Relative humidity ($R^2=0.24$), vapor pressure difference ($R^2=0.14$), and wind speed ($R^2=0.03$) play relatively limited roles. The effects of temperature, on the other hand, are somewhat complex. Except for the cold (warm) summer of 1992 (1998), neither changes in air temperature ($R^2=0.14$) nor surface water temperature ($R^2=0.01$) can explain the interannual variations in evaporation. Similar to the intraseasonal variations, this result appears to be partially due to the competing effects of atmospheric humidity (i.e. years with warm lake temperatures generally coincide with warm air temperatures and, therefore, higher humidity). But perhaps more importantly (given such long timescales), the weak temperature relationship may also reflect the limiting effect of evaporation on surface water temperature. This is corroborated by the fact that interannual changes in evaporation show a strong *negative* relationship with lake–air temperature difference ($R^2=0.61$). We propose that this relationship may provide a simple diagnostic tool for estimating future interannual variations in Sparkling Lake evaporation rates (and perhaps other lakes as well).

An important result of this study is that the effectiveness of the mass transfer formulation depends strongly on the timescale being considered as well as the characteristics of the local wind field. In northern Wisconsin, seasonal temperature variations are large, resulting in a robust relationship between evaporation and vapor pressure difference on seasonal timescales ($R^2=0.92$). The relationship is weaker for the intraseasonal ($R^2=0.46$) and interannual ($R^2=0.14$) timescales, for which temperature variations are considerably reduced. With the exception of Ikebuchi et al. (1988), other studies have also indicated difficulties in applying the mass transfer formula over a wide range of timescales (e.g. Winter, 1981; Sturrock et al., 1992; Sacks et al., 1994).

It is important to note that measurement errors play an important role in the efficacy of the mass transfer formula, particularly considering the smaller variations in atmospheric parameters for the intraseasonal and (especially) interannual timescales. Winter (1981), for example, notes that temperature errors of only 1–2 °C have been found to lead to 25–40% errors in mass transfer evaporation. In the current study, relative humidity should be equally considered, since it is moderately correlated with intraseasonal ($R^2=0.32$) and interannual ($R^2=0.24$) evaporation rates and, at the same time, is one of the more problematic measurements (Table 1). Effects of wind speed deserve special mention here, since (to the authors' knowledge) this is the first study which has documented such strong dissimilarities between variations in evaporation and wind speed. Because of the general quiescence of the mid-summer period (July–August), wind speeds in northern Wisconsin (and presumably other mid-latitude locations) tend to be low during the time of year when evaporation is highest. Thus, Sparkling Lake evaporation estimates using the mass transfer formula are actually *less accurate* when wind speed is included. This continues to hold true for interannual changes in evaporation, which show little correspondence with wind speed ($R^2=0.03$). Only at intraseasonal timescales do we find a moderate, positive relationship between evaporation and wind speed ($R^2=0.16$).

In anticipation of future studies, we have continued to monitor the meteorology and energy budget of Sparkling Lake beyond the 10-year period of the current study. The raft was redeployed in May of 1999 after significant renovation of the raft structure and instrumentation. Included in the new instruments is a highly accurate thermistor chain for improved measurements of daily lake temperature, as well as a more accurate and durable air temperature and relative humidity sensor. In addition, hourly covariances are now explicitly accounted for in the calculation of the Bowen ratio. We anticipate that these improvements will help to reduce some of the uncertainties present in the current study and provide an extension of the 1989–1998 data to allow continued long-term monitoring of lake evaporation. Furthermore, the new raft has been allowed to remain on the lake during the entire year (rather than being

removed during the winter season). This has provided a wealth of new information on the lake energy budget during previously unstudied portions of the year, from late fall to early spring (including the critical periods of ice formation and break up). It is hoped that this new data will improve our understanding of the effects of climate on lake evaporation during times of the year when the lake may be especially sensitive to the effects of climate change.

Acknowledgements

The authors gratefully acknowledge Tim Meinke (UW Trout Lake station) for his valuable assistance in maintaining the raft structure, instrumentation, and data acquisition during an extensive portion of this field project. We also thank Barbara Benson and David Balsiger (UW Center for Limnology) for providing help with data management and processing. The assistance of Tom Winter regarding the initial design of the raft (which is modeled after the Mirror Lake study) is also gratefully acknowledged. Supplementary meteorological data were provided through the University of Wisconsin Automated Weather Observation Network (AWON), while groundwater temperature data were provided by the USGS through David Hamilton. The majority of this project was completed while the first author was a postdoctoral research associate with the Center for Limnology and Center for Sustainability and the Global Environment (SAGE) at the University of Wisconsin-Madison. Funding was provided by the North Temperate Lakes LTER Program (NSF contract DEB-963-2853), a NASA Interdisciplinary Science Investigation (IDS; contract NAG5-3513), and the NASA Upper Midwest RESAC (NAG13-99008). The lake evaporation data and ancillary datasets are publicly available through the NTL-LTER project (<http://lter.limnology.wisc.edu>).

References

- Angel, J.R., Isard, S.A., 1998. The frequency and intensity of great lake cyclones. *Journal of Climate* 11 (1), 61–71.
- Assouline, S., Mahrer, Y., 1993. Evaporation from lake Kinneret. I. Eddy-Correlation system measurements and energy budget estimates. *Water Resources Research* 29 (4), 901–910.
- Attig, J.W., 1985. Pleistocene Geology of Vilas County, Wisconsin. Wisconsin Geological and Natural History Survey, Madison, WI.
- Blanken, P.D., Rouse, W.R., Culf, A.D., Spence, C., Boudreau, L.D., Jasper, J.N., Kochtubajda, B., Scertzer, W.M., Marsh, P., Verseghy, D., 2000. Eddy covariance measurements of evaporation from Great Slave Lake, Northwest Territories, Canada. *Water Resources Research* 36 (4), 1069–1077.
- Blodgett, T.A., Lenters, J.D., Isacks, B.L., 1997. Constraints on the origin of paleolake expansions in the Central Andes. *Earth Interactions* 1.
- Brutsaert, W., 1982. *Evaporation into the Atmosphere*. D. Reidel, Dordrecht. 299 pp.
- Budyko, M.I., 1974. *Climate and Life*. Academic Press, New York. 508 pp.
- Crow, F.R., Hottman, S.D., 1973. Network density of temperature profile stations and its influence on the accuracy of lake evaporation calculations. *Water Resources Research* 9 (4), 895–899.
- dos Reis, R.J., Dias, N.L., 1998. Multi-season lake evaporation: energy-budget estimates and CRLE model assessment with limited meteorological observations. *Journal of Hydrology* 208 (3–4), 135–147.
- Edinger, J.E., Duttweiler, D.W., Geyer, J.C., 1968. The response of water temperatures to meteorological conditions. *Water Resources Research* 4 (5), 1137–1143.
- Gibson, J.J., 2002. Short-term evaporation and water budget comparisons in shallow Arctic lakes using non-steady isotope mass balance. *Journal of Hydrology* 264 (1–4), 242–261.
- Greenland, D., Kittel, T.G.F., 2002. Temporal variability of climate at the US Long-Term Ecological Research (LTER) sites. *Climate Research* 19 (3), 213–231.
- Hagerthey, S.E., Kerfoot, W.C., 1998. Groundwater flow influences the biomass and nutrient ratios of epibenthic algae in a north temperate seepage lake. *Limnology and Oceanography* 43 (6), 1227–1242.
- Hamilton, D.P., De Stasio, B.T., 1997. Modelling phytoplankton-zooplankton interactions in Sparkling Lake, USA. *Verhandlungen Internationale Vereinigung für Limnologie* 26 (2), 487–490.
- Hondzo, M., Stefan, H.G., 1993. Regional water temperature characteristics of lakes subjected to climate-change. *Climatic Change* 24 (3), 187–211.
- Hostetler, S.W., Bartlein, P.J., 1990. Simulation of lake evaporation with application to modeling lake level variations of Harney-Malheur Lake, Oregon. *Water Resources Research* 26 (10), 2603–2612.
- Ikebuchi, S., Seki, M., Ohtoh, A., 1988. Evaporation from lake Biwa. *Journal of Hydrology* 102, 427–449.
- Krabbenhof, D.P., Webster, K.E., 1995. Transient hydrogeological controls on the chemistry of a seepage lake. *Water Resources Research* 31, 2295–2305.
- Krabbenhof, D.P., Anderson, M.P., Bowser, C.J., 1990a. Estimating groundwater exchange with lakes. 2. Calibration of a 3-dimensional, solute transport model to a stable isotope plume. *Water Resources Research* 26 (10), 2455–2462.

- Krabbenhoft, D.P., Bowser, C.J., Anderson, M.P., Valley, J.W., 1990b. Estimating groundwater exchange with lakes. 1. The stable isotope mass balance method. *Water Resources Research* 26, 2445–2453.
- Krabbenhoft, D.P., Anderson, M.P., Bowser, C.J., 1992. Estimating groundwater exchange with lakes. 1. The stable isotope mass balance method and estimating groundwater exchange with lakes. 2. Calibration of a 3-dimensional, solute transport model to a stable isotope plume-reply. *Water Resources Research* 28 (6), 1751–1753.
- Laird, N.F., Kristovich, D.A.R., 2002. Variations of sensible and latent heat fluxes from a great lakes buoy and associated synoptic weather patterns. *Journal of Hydrometeorology* 3 (1), 3–12.
- Likens, G.E., Johnson, N.M., 1969. Measurement and analysis of the annual heat budget for the sediments in two Wisconsin lakes. *Limnology and Oceanography* 14, 115–135.
- Livingstone, D.M., Dokulil, M.T., 2001. Eighty years of spatially coherent Austrian lake surface temperatures and their relationship to regional air temperature and the North Atlantic Oscillation. *Limnology and Oceanography* 46 (5), 1220–1227.
- Magnuson, J.J., Bowser, C.J., 1990. A network for long-term ecological research in the United States. *Freshwater Biology* 23 (1), 137–143.
- Magnuson, J.J., Kratz, T.F., Allen, T.F.H., Armstrong, D.E., Benson, B.J., Bowser, C.J., Bolgrien, D.W., Carpenter, S.R., Frost, T.M., Gower, S.T., Lillesand, T.M., Pike, J.A., Turner, M.G., 1997. Regionalization of long-term ecological research (LTER) on north temperate lakes. *Verhandlungen Internationale Vereinigung für Limnologie* 26 (2), 522–528.
- Mohseni, O., Stefan, H.G., 1999. Stream temperature air temperature relationship: a physical interpretation. *Journal of Hydrology* 218 (3–4), 128–141.
- Morton, F.I., 1983a. Operational estimates of areal evapotranspiration and their significance to the science and practice of hydrology. *Journal of Hydrology* 66, 1–76.
- Morton, F.I., 1983b. Operational estimates of lake evaporation. *Journal of Hydrology* 66, 77–100.
- Morton, F.I., 1986. Practical estimates of lake evaporation. *Journal of Climate and Applied Meteorology* 25, 371–387.
- Myrup, L.O., Powell, T.M., Godden, D.A., Goldman, C.R., 1979. Climatological estimate of the average monthly energy and water budgets of Lake Tahoe, California-Nevada. *Water Resources Research* 15 (6), 1499–1508.
- Peeters, F., Livingstone, D.M., Goudsmit, G.H., Kipfer, R., Forster, R., 2002. Modeling 50 years of historical temperature profiles in a large central European lake. *Limnology and Oceanography* 47 (1), 186–197.
- Robertson, E., Barry, P.J., 1985. The water and energy balances of Perch Lake (1969–1980). *Atmosphere Ocean* 23, 238–253.
- Robock, A., 2002. Pinatubo eruption—the climatic aftermath. *Science* 295 (5558), 1242–1244.
- Robock, A., Mao, J.P., 1995. The volcanic signal in surface-temperature observations. *Journal of Climate* 8 (5), 1086–1103.
- Rogers, C.K., Lawrence, G.A., Hamblin, P.F., 1995. Observations and numerical simulation of a shallow ice-covered midlatitude lake. *Limnology and Oceanography* 40 (2), 374–385.
- Rosenberry, D.O., Sturrock, A.M., Winter, T.C., 1993. Evaluation of the energy budget method of determining evaporation at Williams Lake, Minnesota, using alternative instrumentation and study approaches. *Water Resources Research* 29 (8), 2473–2483.
- Sacks, L.A., Lee, T.M., Radell, M.J., 1994. Comparison of energy-budget evaporation losses from two morphometrically different Florida seepage lakes. *Journal of Hydrology* 156, 311–334.
- Schindler, D.W., 2001. The cumulative effects of climate warming and other human stresses on Canadian freshwaters in the new millennium. *Canadian Journal of Fisheries and Aquatic Sciences* 58 (1), 18–29.
- Sene, K.J., Gash, J.H.C., McNeil, D.D., 1991. Evaporation from a tropical lake: comparison of theory with direct measurements. *Journal of Hydrology* 127, 193–217.
- Stannard, D.I., Rosenberry, D.O., 1991. A comparison of short-term measurements of lake evaporation using eddy correlation and energy budget methods. *Journal of Hydrology* 122, 15–22.
- Stauffer, R.E., 1991. Testing lake energy budget models under varying atmospheric stability conditions. *Journal of Hydrology* 128, 115–135.
- Stauffer, R.E., 1992. Comment on “estimating groundwater exchange with lakes. 1. The stable isotope mass balance method” and “estimating groundwater exchange with lakes. 2. Calibration of a three-dimensional, solute transport model to a stable isotope plume” by David P. Krabbenhoft et al. *Water Resources Research* 28 (6), 1747–1749.
- Sturrock, A.M., Winter, T.C., Rosenberry, D.O., 1992. Energy budget evaporation from Williams lake—a closed lake in North Central Minnesota. *Water Resources Research* 28 (6), 1605–1617.
- Vallet-Coulomb, C., Legesse, D., Gasse, F., Travi, Y., Chernet, T., 2001. Lake evaporation estimates in tropical Africa (Lake Ziway, Ethiopia). *Journal of Hydrology* 245 (1–4), 1–18.
- Webb, E.K., 1960. On estimating evaporation with fluctuating Bowen ratio. *Journal of Geophysical Research* 65 (10), 3415–3417.
- Webb, E.K., 1964. Further note on evaporation with fluctuating Bowen ratio. *Journal of Geophysical Research* 69 (12), 2649–2650.
- Winter, T.C., 1981. Uncertainties in estimating the water balance of lakes. *Water Resources Bulletin* 17 (1), 82–115.
- Winter, T.C., Rosenberry, D.O., Sturrock, A.M., 1995. Evaluation of 11 equations for determining evaporation for a small lake in north central United States. *Water Resources Research* 31, 983–993.
- Winter, T.C., Buso, D.C., Rosenberry, D.O., Likens, G.E., Sturrock, A.M., Mau, D.P., 2003. Evaporation determined by the energy-budget method for Mirror Lake, New Hampshire. *Limnology and Oceanography* 48 (3), 995–1009.
- Yu, Y.S., Knapp, H.V., 1985. Weekly, monthly, and annual evaporations for Elk City Lake. *Journal of Hydrology* 80, 93–110.